Rare Met.
https://doi.org/10.1007/s12598-022-02058-2

RARE METALS

REVIEW

Ti_3C_2 MXene: recent progress in its fundamentals, synthesis, and applications

Wei-Xin Huang, Zhi-Peng Li, Dong-Dong Li, Zhi-Hui Hu, Chao Wu, Kang-Le Lv, Qin Li*

Received: 3 December 2021 / Revised: 9 January 2022 / Accepted: 23 January 2022

Abstract In this rapidly developing society, it is always crucial to exploit new materials with suitable properties to meet specific application demands. Two-dimensional (2D) transition metal carbon/nitrides (MXenes) are a novel graphene-like material with exciting research potential in recent years. Among them, Ti_3C_2 debuts in a central position due to its relatively longer research history, mature synthetic process, and incredibly rich store of merits, such as good flexibility, large specific surface area, abundant termination groups, excellent electrical conductivity, and light-to-heat conversion ability. In this review, recent research progress on Ti_3C_2 MXene and its composites was updated mainly from three aspects, including their fundamentals, synthesis, and applications. It has been found that diverse applications of Ti_3C_2-based composites are inseparable and correlated with each other, which were linked by their unique physicochemical properties. In the end, a summary and a perspective on future opportunities and challenges of Ti_3C_2 were given to offer theoretical and technical guidelines for further investigation on MXene family.

Keywords Ti_3C_2 MXene; Delamination; Biomedicine; Battery and supercapacitor; Sensor; Photocatalyst

W.-X. Huang, Z.-P. Li, Z.-H. Hu, C. Wu, K.-L. Lv, Q. Li*
South-Central Minzu University, Wuhan 430074, China
e-mail: liqin0518@mail.scuec.edu.cn

D.-D. Li
Wuhan Research Institute of Materials Protection, Wuhan 430000, China

1 Introduction

Since the single-layer graphene was amazedly acquired from graphite by a stripping method in 2004 [1], its unique electrochemical and optoelectronic properties excited a huge research enthusiasm on the fabrication and exfoliation of two-dimensional (2D) layered materials, such as silicone [2], germanene [3], phosphorene [4], MoS_2 [5], and clays [6]. In 2011, Naguib et al. [7] originally extracted the Al layers from Ti_3AlC_2 by hydrofluoric acid (HF) to form a novel laminated Ti_3C_2 nanocrystal, which owned graphene-like properties and morphology and therefore was defined as "MXene." Thereafter, more transition metal carbides and/or nitrides such as Ti_2C, Ti_3C_2, Ti_3CN, Ta_4C_3, Nb_2C, Nb_4C_3 and V_2C were discovered to extensively expand this burgeoning MXene family [8–10]. The general formula of MXene is $M_{n+1}X_nT_x$ (n = 1–3), in which M means early transition metals (i.e., Sc, Ti, V, Cr, Zr, Hf, Nb, Mo, Ta, and W), X stands for carbon and/or nitrogen, and T_x refers to the surface terminations (such as –OH, –O, and –F) which was formed during the chemical etching process [11]. The originally obtained MXene from its MAX phase usually appears as an accordion-like structure, which is not only conducive to the interpenetration of ions for specific applications (such as batteries and sensors), but also highly flexible and shapeable, because single- or few-layer form of MXenes can be readily obtained by a facile delamination step from their accordion-like multilayer form [12–16], and even more, quantum dot (QD) form of MXenes can also be achieved by further treatment such as hydro-/solvothermal [17, 18], ball milling [19] and micro-explosion [20] strategies.

Although the MXene family was continually expanding with the assistance of both theoretical and experimental

Published online: 03 August 2022

technologies, $Ti_3C_2T_x$ still debuts in a central role among the MXenes up to now for the following reasons. (1) The preparation process of $Ti_3C_2T_x$ is simple and low-cost with a wide market prospect [21]. (2) $Ti_3C_2T_x$ is fairly flexible in various structures including three-dimensional (3D) accordion-like multilayers, 2D lamellar nanosheets, and zero-dimensional (0D) ultra-small QDs, which can meet different requirements in diverse situations [22]. (3) The electronic energy band structure and physicochemical properties of $Ti_3C_2T_x$ are feasibly steerable by controlling the abundant functional groups on its surface [23]. (4) Apart from the terminations on the surface, local defects also exist in $Ti_3C_2T_x$, which can be fully utilized in the preparation of MXene-based composites [24]. (5) $Ti_3C_2T_x$ exhibited outstanding electrical conductivity even with the surface terminations and local defects [25]. (6) In $Ti_3C_2T_x$, carbon is the basic element for constructing living organism, and transition metal Ti is inert to living beings. Therefore, $Ti_3C_2T_x$ is non-toxic and biodegradable, which has unparalleled research potential in the field of biomedicine [26].

Although $Ti_3C_2T_x$ has multifarious excellent characteristics, there are still some shortcomings that hinder its current development. For example, the structure of $Ti_3C_2T_x$ tends to inevitably collapse in a humid environment, because the exposed Ti atoms on the surface make it easily oxidized. In addition, the synthesis methods to obtain $Ti_3C_2T_x$ were still limited, which usually required the use of hazardous fluorinated reagent [22]. In order to further expand the application areas of $Ti_3C_2T_x$ and accelerate its development pace, researchers have constructed it into hybrids with other materials including metal [25], metal oxide [27], metal sulfide [28], polymer [29], protein [30], and natural organic molecules [31] to combine their merits.

Hitherto, the research on $Ti_3C_2T_x$ and its hybrids is still in its infancy. Thus, it is quite necessary to update the recent research progress and milestones on $Ti_3C_2T_x$ MXene. In this review, we initially introduced the fundamentals of $Ti_3C_2T_x$ MXene, such as their atomic structure, crystal phase, morphologies, and physicochemical properties. Subsequently, we emphasized the synthesis methods of various formed $Ti_3C_2T_x$ and their composites. Next, we summarized the diverse applications of $Ti_3C_2T_x$ in different fields, including energy storage, electromagnetic interference, photothermal conversion, biomedical application, sensor, and photocatalysis. Besides, the synthesis strategies and applications of $Ti_3C_2T_x$-based composites are classified and summarized in Table 1 [15, 19, 24, 25, 28, 29, 31–58]. Meanwhile, as shown in Fig. 1, linked by their unique physicochemical properties, diverse applications of $Ti_3C_2T_x$-based composites are inseparable and correlated with each other, just like the pieces of a jigsaw puzzle. Finally, a perspective on future opportunities and challenges of MXene materials was provided. It aims to offer theoretical and technical guidelines for the preparation and application of $Ti_3C_2T_x$ and other similar MXene materials (Fig. 1).

2 Fundamentals

In-depth understanding and research on the fundamentals of $Ti_3C_2T_x$ are not only instructive to promoting its fabrication strategy, but also conducive to discovering and extending its great potential in various fields. Therefore, in this part, we will demonstrate its fundamentals from the aspects of atomic structure, crystal phase, morphology, and various physicochemical properties in detail.

2.1 Atomic structure and crystal phase

To understand the atomic structure of Ti_3C_2 MXene, one must retrospect its precursor, Ti_3AlC_2 MAX. As shown in Fig. 2a, the crystal structure of Ti_3AlC_2 involves the periodic superposition of six atomic layers (Ti–C–Ti–C–Ti–Al) along its cross section [22]. Typically, the Ti layer is closely packed and interleaved with the Al element layer, and C atoms fill the octahedral sites on the Ti layers [11]. Fortunately, Ti_3C_2 MXene can be easily prepared from the Ti_3AlC_2 MAX by selectively removing "Al" layer through etching methods, because Ti–C bound layers with metallic bond energy are more stable than Ti–Al layers [7, 13, 59]. After the etching treatment, the exposed metal sites on Ti_3C_2 surface have higher redox activity than the carbon sites in the framework. Thereby, the bare Ti_3C_2 possesses high surface energy and prefers to quickly react with the anions in the solution to form the functional terminations, such as –O, –OH, and/or –F, which were noted as T_x, where x is the number of the terminal groups [12, 60].

Technically, X-ray diffraction (XRD) analysis could tell the transition of the crystal phases from Ti_3AlC_2 MAX to Ti_3C_2 MXene. As displayed in Fig. 2b, XRD pattern of the initial Ti_3AlC_2 shows a spiculate (104) diffraction peak at $2\theta \approx 39°$, as well as other typical diffraction peaks, such as those at the 2θ values of 9.4°and 19.0°, which correspond to (002) and (004) crystal planes, respectively [13]. These characteristic peaks all confirmed the hexagonal crystal phase of Ti_3AlC_2. The etching of Al elements from Ti_3AlC_2 to form Ti_3C_2 was evidenced by the disappearance of the (104) peak, as well as the shift of (002) and (004) peaks to a lower angle [36]. At the same time, the diffraction peaks of (002) and (004) were obviously broadened and weakened, which indicated that the interplanar spacing between the Ti_3C_2 multilayers became larger and thus, the c-lattice parameter (c-LP) increased [12]. Nevertheless, the selected area electron diffraction (SAED)

Table 1 Summary of synthetic approaches and applications of Ti_3C_2-based composites

Nos.	Ti_3C_2-based composites	Synthetic approach	Morphology of Ti_3C_2 in composite	Application	Refs.
1	(111)TiO_{2-x}/Ti_3C_2	Hydrothermal	Multilayer	Photocatalytic pollutant degradation	[33]
2	$Cu_y/TiO_2@Ti_3C_2T_x$	Hydrothermal	Multilayer	Photocatalytic; H_2 production	[34]
3	$Zn_2In_2S_5/Ti_3C_2$	Hydrothermal	Multilayer	Photocatalytic; H_2 production	[35]
4	Bi_2WO_6/Ti_3C_2	Hydrothermal	Monolayer	Photocatalytic; CO_2 reduction	[36]
5	Cu_3BiS_3/Ti_3C_2	Hydrothermal	Monolayer	Photothermal conversion	[32]
6	CdS/Ti_3C_2	Hydrothermal	Quantum dot	Photocatalytic; H_2 production	[37]
7	$ZnIn_2S_4/Ti_3C_2$	Solvothermal	Monolayer	Photocatalytic; H_2 production	[28]
8	$Cds@Au/Ti_3C_2$	Solvothermal	Monolayer	Photocatalytic; H_2 production	[24]
9	Co_3O_4/Ti_3C_2	Solvothermal	Monolayer	Photothermal conversion	[40]
10	$Zn@Ti_3C_2$	Deposition	Multilayer	Supercapacitor	[38]
11	$Ti_3C_2T_x$/carbon nanotubes (CNTs)	Chemical vapor deposition	Multilayer	Electromagnetic; Wave absorption	[41]
12	LTO (lithiophilic)/Ti_3C_2	Electrochemical deposition	Multilayer	Battery	[42]
13	$Ti_3C_2T_x$/CNTs	Electrostatic self-assembly	Monolayer	Supercapacitor	[43]
14	$Ti_3C_2T_x$-rGO	Electrostatic self-assembly	Monolayer	Supercapacitor	[44]
15	PANI (positively charged conductive polyaniline)/$Ti_3C_2T_x$	Electrostatic self-assembly	Monolayer	Battery	[45]
16	Ti_3C_2/S-ENR (serine-grafted epoxidized natural rubber)	Self-assembly	Monolayer	Sensor	[46]
17	Ti_3C_2/polyelectrolyte	Layer-by-layer (LBL); self-assembly	Monolayer	Sensor	[29]
18	Ti_3C_2/CNT	LBL; self-assembly	Monolayer	Electromagnetic interference shielding	[47]
19	Ti_3C_2 QDs/Cu_2O nanowires (NWs)/Cu	Self-assembly	Quantum dot	Photocatalytic; CO_2 reduction	[39]
20	$TiO_2/C_3N_4/Ti_3C_2$ QDs	Self-assembly	Quantum dot	Photocatalytic; CO_2 reduction	[48]
21	(001)$TiO_2/Ti_3C_2T_x$	In situ grown	Multilayer	Photocatalytic pollutant degradation	[58]
22	TiO_2/Ti_3C_2	In situ grown	Multilayer	Photocatalytic; CO_2 reduction	[50]
23	Ti_3C_2-IONPs@PEG (iron oxide nanoparticles@ amino-[poly(ethylene -glycol)])	In situ grown	Monolayer	Biomedicine	[51]
24	MXene/Ag	Self-reduction	Multilayer	Battery	[52]
25	$Pt_1/Ti_3C_2T_x$	Self-reduction	Monolayer	Single-atom catalyst	[25]
26	Ti_3C_2/graphene oxide	Freeze-drying	Monolayer	Battery	[53]
27	Ti_3C_2/NMC (natural microcapsule)	Vacuum-assisted filtration	Multilayer	Sensor	[31]

Table 1 continued

Nos.	Ti_3C_2-based composites	Synthetic approach	Morphology of Ti_3C_2 in composite	Application	Refs.
28	Ti_3C_2/AgNWs (silver nanowires)	Vacuum-assisted filtration	Monolayer	Supercapacitor	[54]
29	BCs (bacterial cellulose)/Ti_3C_2	Vacuum-assisted filtration	Monolayer	Electromagnetic interference shielding	[55]
30	$Ti_3C_2T_x$/Nb_2CT_x	Vacuum-assisted filtration	Monolayer	Sensor	[56]
31	CNF (cellulose nanofibers)/Ti_3C_2/BCs	Hot press	Monolayer	Electromagnetic interference shielding	[57]
32	MXene/DOX (doxorubicin)@cellulose	Chemical; cross-linking	Monolayer	Biomedicine	[49]
33	TNDs ($Ti_3C_2T_x$ nanodots)/P (red phosphorous)	Ball milling	Quantum dot	Battery	[19]
34	Ti_3C_2/g-C_3N_4	Calcination	Monolayer	Photocatalytic; CO_2 reduction	[15]

pattern of few-layer Ti_3C_2 shows the typical hexagonal diffraction pattern (inset in Fig. 2c), indicating that the quality of the Ti_3C_2 nanosheets is intact and the hexagonal structure is still maintained after peeling off [38].

2.2 Morphology

Obviously, the macro- and micro-appearance of Ti_3AlC_2 will change dramatically after being etched into $Ti_3C_2T_x$. From a macro-perspective, the dense powder became fluffy, and its color changed from black to dark purple or bright black (Fig. 3a, b). Microscopically, it can be observed from scanning electron microscopy (SEM) image that the bulk Ti_3AlC_2 exhibited a compact layered structure (Fig. 3c), while $Ti_3C_2T_x$ presented an accordion-like shape (Fig. 3d) [8]. Through some specific treatment (see Sect. 3.2), the accordion $Ti_3C_2T_x$ could be peeled off to form 2D single-layer nanosheets, which are more favored by researchers due to its larger specific surface area and unique quantum size effect. In reality, the tested thickness of $Ti_3C_2T_x$ nanosheets by atomic force microscope (AFM) technique was usually 0.5–2.0 nm with the presence of surface groups and absorbed water molecules [61–65]. For example, Lipatov et al. [16] prepared monolayer $Ti_3C_2T_x$ (Fig. 3e), and the AFM height curve in Fig. 3f shows that it was about 1.5 nm in thickness. Similar results have also been reported in other studies related to $Ti_3C_2T_x$, where the thicknesses were tested as 0.74, 0.98 and 1.63 nm, respectively [65–68].

For the lamellar size of $Ti_3C_2T_x$ monolayer, it varies along with the utilized preparation methods. For instance, the $Ti_3C_2T_x$ monolayer flakes prepared by a harsh chemical corrosion method in 40% HF aqueous solution were usually broken down to nanometer level in lamellar size (100–400 nm) [69]. In comparison, those prepared in milder conditions such as LiF/HCl and NH_4Cl etching methods often possess much larger size in micrometer level [70]. Generally, the larger the lamellar size of nanosheets is, the more the active sites are exposed. However, sometimes, small flakes are also in demand due to their agility. Especially, $Ti_3C_2T_x$ QDs can be prepared by proper methods such as hydro-/solvothermal [17, 18, 39], ball milling [19], and micro-explosion [20] strategies. As shown in Fig. 3g, h, $Ti_3C_2T_x$ QDs with the lattice spacing of 0.21 nm are relatively uniform in size, and the average size is less than 10 nm [10].

2.3 Physicochemical properties

As a new member of 2D materials, Ti_3C_2 MXene with a regular metal atom skeleton displays some unique properties. With the assistance of abundant surface functional groups on Ti_3C_2, the obtained $Ti_3C_2T_x$ can perfectly combine the metal conductivity and the hydrophilicity [10, 59]. Moreover, specific characteristics of $Ti_3C_2T_x$ can be achieved by controlling and adjusting these terminal functional groups, which is of great research value.

In this part, three typical physicochemical properties of $Ti_3C_2T_x$ including electrical conductivity, hydrophilicity, and mechanical stability will be introduced in detail to further recognize its fundamentals.

2.3.1 Electrical conductivity

Undeniably, one of the most critical factors that motivate researchers to keep enthusiastic in the research of $Ti_3C_2T_x$ is its unparalleled conductivity. It is the conductive carbide core along with transition metal oxide-like surfaces that

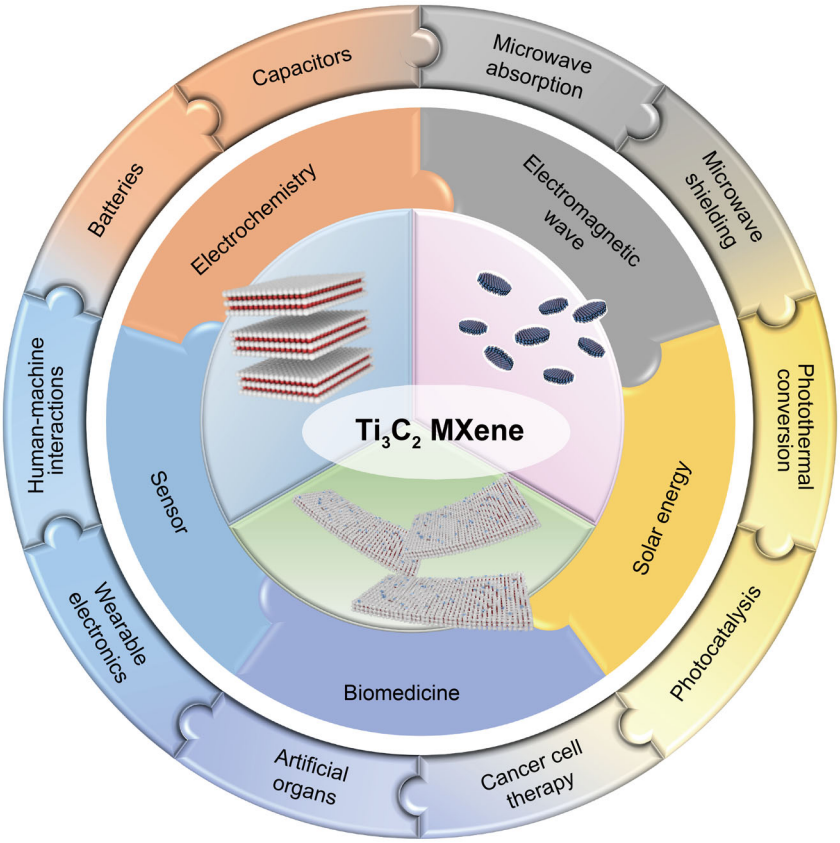

Fig. 1 Schematic diagram of applications of different dimensional $Ti_3C_2T_x$ MXene in diverse and correlative fields

plays a central role in the electrical conductivity of $Ti_3C_2T_x$ [71]. It has been reported that a pure $Ti_3C_2T_x$ MXene film with a thickness of 940 nm prepared by a scalable blade coating process using large-sized MXene flakes can exhibit the electrical conductivity up to $\approx$ 15,100 S·cm^{-1} [72]. Compared with the conductivity of graphene films (1.5×10^4 S·cm^{-1}) [73], the conductivity of $Ti_3C_2T_x$ is in the same order of magnitude. Therefore, it is supposed to be a promising alternative to graphene.

The electrical conductivity of $Ti_3C_2T_x$ is usually influenced by the factors including terminal groups [74], interlamellar spacing between flakes, and ambient temperature. Firstly, the electrical conductivity of $Ti_3C_2T_x$ can be distinctly improved by removing part of the surface functional groups via annealing in vacuum [75]. For example, Wang et al. [23] roasted $Ti_3C_2T_x$ nanosheets at 600 °C for 1 h, and successfully reduced the amount of the functional groups to shorten the conduction path of electrons, which resulted in the enhancement of its conductivity by nearly three times. Secondly, increasing the interlamellar spacing between the flakes influences the electrical properties of $Ti_3C_2T_x$. For instance, the conductivity of multilayer $Ti_3C_2T_x$ was reported to be one order of magnitude lower than that of single-layer one ((4600 $\pm$ 1100) S·cm^{-1}) [16]. Furthermore, the used intercalants to increase the interlayer spacing of the multilayered $Ti_3C_2T_x$ also decreased its resistivity. For instance, Muckley et al. [76] reported that H_2O and Li^+ intercalation caused the resistance value of $Ti_3C_2T_x$ to decrease from 41 to 10 Ω. Thirdly, temperature is also a vital effect for the electron conductivity of $Ti_3C_2T_x$ MXene. For example, Halim et al. [77] and Bergmann [78] confirmed that the resistivity of the 2D $Ti_3C_2T_x$ nanofilm increases from 4.8 to 6.1 μΩ·m with the decrease in temperature when the temperature is below 100 K, which is attributed to the common electron backscattering phenomenon in 2D metals materials.

The feature of good electro-conductivity has now been used as the most dazzling advantage of $Ti_3C_2T_x$ in various fields including electromagnetic wave absorption and shielding, energy conversion, sensors, catalysis, etc. Thereby, more efforts should be invested in the development and optimization of the MXene's conductivity.

2.3.2 Hydrophilicity and hydrophobicity

$Ti_3C_2T_x$ MXene was usually derived by the acid etching process in a watery environment, thus abundant polar terminal groups were formed on its surface. These

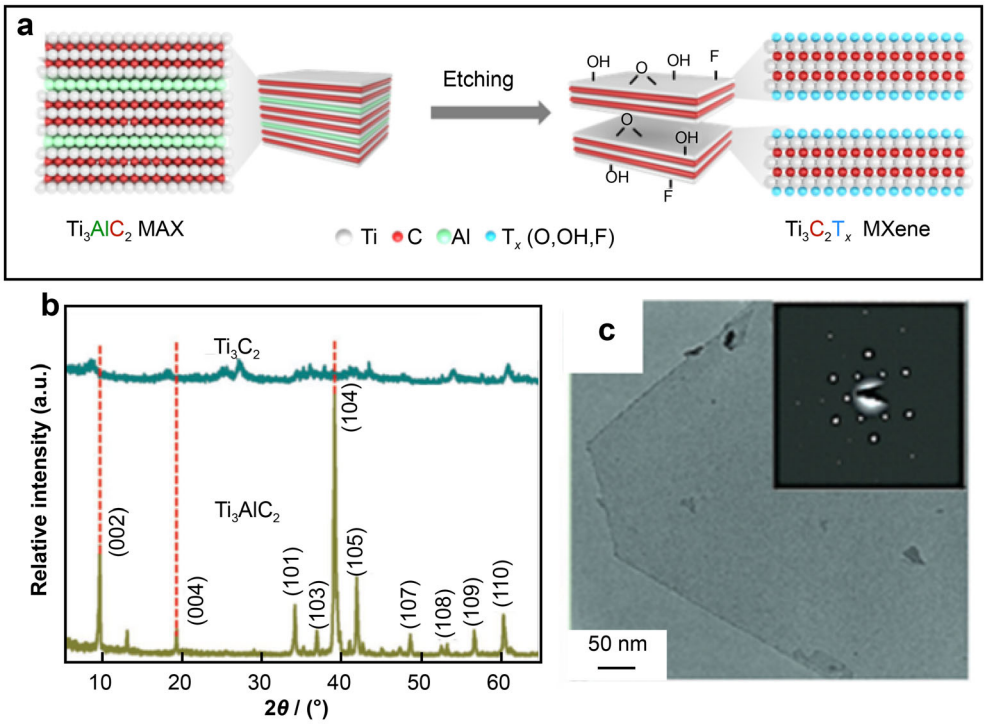

Fig. 2 Atomic structure of Ti_3C_2 MXene. **a** Scheme of $Ti_3C_2T_x$ MXene formation from Al etching in Ti_3AlC_2 MAX; **b** comparison of XRD patterns of Ti_3AlC_2 and Ti_3C_2. Reproduced with permission from Ref. [36]. Copyright 2018, Wiley. **c** TEM image of Ti_3C_2 nanoflakes and (inset) its corresponding SAED pattern. Reproduced with permission from Ref. [16]. Copyright 2016, Wiley

terminations always resulted in strong hydrophilicity of $Ti_3C_2T_x$ nanosheets, which has been taken full advantage in some typical application fields, such as photocatalytic pollutant degradation, biomedicine, and seawater desalination. For instance, Cai et al. [79] made full use of the abundant hydrophilic functional groups on the surface of $Ti_3C_2T_x$ to form a strong interface contact with Ag_3PO_4 to promote the separation of electron–hole pairs and achieve high-efficiency photocatalytic degradation of organic pollutants. Furthermore, Singh et al. [80] confirmed that $Ti_3C_2T_x$ featured with good hydrophilicity showed excellent cell adhesion to mouse fibroblasts, which exhibited good biocompatibility. In addition, Zhang et al. [81] designed an amphiphilic MXene aerogel for solar desalination by vertically arranged $Ti_3C_2T_x$, where the upper layer was hydrophobic, and the bottom layer was hydrophilic. The designed aerogel was featured with adjustable and ordered vertical-array structure, which achieved a daily seawater output of 6 $L{\cdot}m^{-2}$ due to the feasibility of steam escape, moisture transfer, and little heat loss.

On the other hand, a hydrophobic surface of $Ti_3C_2T_x$ suitable for specific environments can also be obtained by adjusting its surface functional terminations or introducing it into other functional materials to construct composites [82]. For example, Zhao et al. [83] prepared a hydrophobic $Ti_3C_2T_x$ MXene film terminated with trimethoxy groups for solar steam conversion. The efficiency reached 71%, ensuring efficient and long-term stable light and heat transmission in seawater with high salinity. In addition, Liu et al. [84] prepared hydrophobic porous Ti_3C_2-based foam by fixing the Ti_3C_2 film between two ceramic wafers, which were coated with 80% hydrazine monohydrate and then calcined in 90 °C. Compared with the hydrophilic Ti_3C_2 films with a contact angle of 59.5°, the Ti_3C_2-based foam exhibited hydrophobic character with a contact angle of 94.0°. The unique hydrophobicity-made Ti_3C_2 foam possessed excellent durability in humid environments and also improved its stability in water.

Although the abundant surface terminal groups endow $Ti_3C_2T_x$ MXene with excellent hydrophilic characteristics, it is easily oxidized by the air or water to form TiO_2, and subsequently results in the structure collapse of $Ti_3C_2T_x$, which is a non-negligible issue hindering the further development and wide application scope of MXene-based materials. Up to now, many researchers have taken effort to tackle this problem by various methods such as saving in organic antioxidant, isolating from oxygen, and refrigerating in a low temperature. For instance, Zhao et al. [85] utilized sodium L-ascorbate (NaAsc) as an antioxidant to prevent the oxidation of $Ti_3C_2T_x$ nanosheets in wet environments. The L-ascorbate group could associate with the

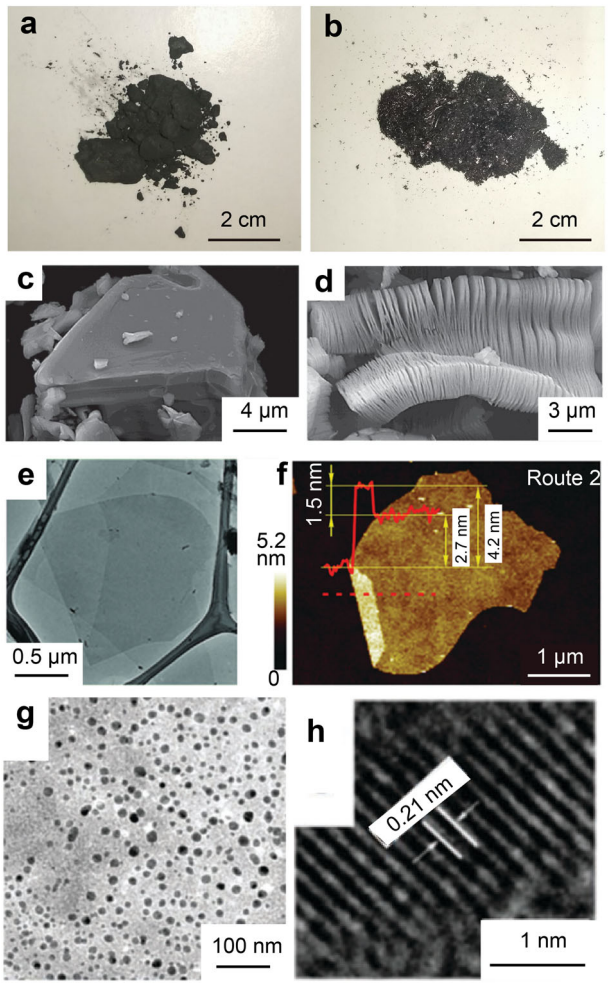

Fig. 3 Morphology of Ti_3C_2 MXene. Photographs of **a** Ti_3AlC_2 MAX powder and **b** Ti_3C_2 MXene powder; SEM images of **c** Ti_3AlC_2 precursor and **d** 3D Ti_3C_2 multilayers. Reproduced with permission from Ref. [8]. Copyright 2012, American Chemical Society. **e** TEM and **f** AFM images of 2D $Ti_3C_2T_x$ monolayers. Reproduced with permission from Ref. [16]. Copyright 2016, Wiley. **g** TEM and **h** HRTEM images of 0D $Ti_3C_2T_x$ QDs. Reproduced with permission from Ref. [10]. Copyright 2018, The Royal Society of Chemistry

terminations of $Ti_3C_2T_x$ to restricting their further reactions with water in colloidal solution. The as-obtained $Ti_3C_2T_x$ sheets retained its inchoate morphology after even half a year. Analogously, dimethyl sulfoxide (DMSO), ethanol, and n-picoline have also been proven to prolong the lifetime of $Ti_3C_2T_x$ to ca. ~ 30 days [86]. However, the utilized organic additives will inevitably remain in the $Ti_3C_2T_x$ layers and cause the decreased conductivity. Moreover, in order to remove these organic reagents, the exposure time of MXene to water and air will be increased. For long-term storage of $Ti_3C_2T_x$, the more direct and effective method is to store it in powder form under vacuum [87], or to inject inert gas into the solution to isolate the MXene from water and/or oxygen [88]. Furthermore, Habib et al. [89] recently verified that $Ti_3C_2T_x$ oxidized fastest in liquid media and slowest in solid media (including polymer matrix). Thereafter, Zhang et al. [87] proposed that freezing the MXene aqueous dispersion at − 20 °C could effectively prevent the formation of TiO_2 nanoparticles on the edge of $Ti_3C_2T_x$ in the early stage of oxidation.

2.3.3 Mechanical stability

Mechanical stability of equipment and devices has become a key consideration in their practical applications. So far, due to the excellent mechanical stability, $Ti_3C_2T_x$ nanosheet has been proven to be one of the chosen materials for the next generation of flexible functional devices [90, 91]. The mechanical properties of Ti_3C_2 nanosheets largely depend on the interaction force between individual nanosheets. When the thickness of the $Ti_3C_2T_x$ film is 940 nm, the tensile strength can reach 570 MPa, and the corresponding Young's modulus in the vertical direction is about 20.6 GPa [72]. In order to adapt to the development of intelligent technology, reducing the thickness of the product while ensuring its mechanical stability is extremely important for flexible electronic devices. Therefore, the tensile strength of Ti_3C_2 nanosheets with a thickness of about 40 nm optimized by Firestein et al. [92] can be as high as 670 MPa, which can be proved by in situ transmission electron microscopy (TEM) tensile strength testing. Meanwhile, the Young's modulus perpendicular to the direction of the $Ti_3C_2T_x$ nanosheet was measured to be 120–140 GPa. In addition, the ultimate tensile strength (UTS) can be significantly affected by defects in the structure of $Ti_3C_2T_x$. It was reported that when the defect concentration in the structure increased from 2% to 8%, the UTS of $Ti_3C_2T_x$ nanosheets decreased from 21.6 to 18.9 GPa [92]. Therefore, it can be concluded that the mechanical properties of $Ti_3C_2T_x$ can be adjusted by controlling the thickness of the nanosheets and concentration of the structural defects.

3 Synthesis methods

Contemporarily, the chief strategy to obtain Ti_3C_2 MXene is selectively etching Al element layers from the Ti_3AlC_2 MAX phase, which could be obtained by the bottom-up synthesis method from atoms and molecules, such as chemical vapor magnetron sputtering [77] and self-propagating high-temperature synthesis (MASHS) method [93]. To improve the work efficiency, most researchers preferred to directly purchase Ti_3AlC_2 powder from companies, such as Beijing Lianli New Technology Co., Ltd, China [36], Jilin 11 Technology Co., Ltd, China [94], Macklin [28],

and Sinopharm Chemical Reagent Co. Ltd. [79]. In this section, we firstly present the technologies for preparing $Ti_3C_2T_x$ multilayer flakes from Ti_3AlC_2 MAX precursor, and then illustrate the delamination methods of $Ti_3C_2T_x$ to obtain few-layer or single-MXene nanosheets. Subsequently, the synthetic strategies of 2D-nanosheet and 0D-QD MXenes were expounded. At last, the design and fabrication strategies of $Ti_3C_2T_x$-based composites were also summarized.

3.1 Synthesis of $Ti_3C_2T_x$ multilayer flakes

Different from other 2D materials, such as graphene and MoS_2, the force between the MAX layers is much stronger due to the presence of M–A metal bonds [13]. In 2011, Gogotsi et al. unprecedentedly reported that $Ti_3C_2T_x$ multilayer could be produced by selective etching Al atoms from Ti_3AlC_2 MAX phase in 50% hydrofluoric acid (HF) aqueous solution (Fig. 4a) [7]. Typically, when Ti_3AlC_2 is immersed in HF aqueous solution, the etching reaction equations are as follows:

$$Ti_3AlC_2 + 3HF = AlF_3 + 3/2H_2 + Ti_3C_2 \quad (1)$$

$$Ti_3C_2 + 2H_2O = Ti_3C_2(OH)_2 + H_2 \quad (2)$$

$$Ti_3C_2 + 2HF = Ti_3C_2F_2 + H_2 \quad (3)$$

In Eq. (1), Al atoms are exfoliated from the Ti_3AlC_2 MAX phase to form Ti_3C_2. After etching, the exposed Ti atoms will become the reaction sites, which is easy to react with water (Eq. (2)) and HF (Eq. (3)) to produce $Ti_3C_2(OH)_2$ and $Ti_3C_2F_2$, respectively. In most cases, Eqs. (2, 3) occurred simultaneously [7].

However, HF is a dangerous and toxic substance due to that it is strongly corrosive and irritating effect to the skin, eyes, and respiratory tract. Alternatively, a LiF/HCl mixed solution was then developed as a milder etchant. As illustrated in Eq. (4), the HF species with a controllable concentration can be in situ produced from LiF and HCl, and serve as the etchant for Ti_3AlC_2. Interestingly, it has been found that the $Ti_3C_2T_x$ MXene produced by this mild etching method usually possessed a larger planar size and fewer atomic defects than that produced by HF etching [95]. Similarity, Wang et al. [96] employed NH_4F to remove Al element from bulk Ti_3AlC_2 for preparing multilayered Ti_3C_2 by a facial hydrothermal strategy. Followed Eqs. (5, 6), this method also avoids the direct utilization of HF.

$$LiF + HCl = HF + LiCl \quad (4)$$

$$NH_4F + H_2O = NH_3 \cdot H_2O + HF \quad (5)$$

$$3NH_4F + AlF_3 = (NH_4)_3AlF_6 \quad (6)$$

Although the optimized LiF/HCl etching method avoids the direct utilization of HF, danger is still not changed in essence. Therefore, Feng et al. [97] attempted to use XHF_2 (where X presents K^+, Na^+, NH_4^+) to replace HF as the etchant for the production of $Ti_3C_2T_x$ based on Eq. (7) (Fig. 4b). Therein, NH_4HF_2 allows extra intercalation of NH^{4+} cations and NH_3 molecules in the etching reactions. In this way, $Ti_3C_2T_x$ can be obtained in a single reaction with a large interplanar spacing, so the accordion structure can be better maintained.

$$Ti_3AlC_2 + XHF_2 = X_aAlF_b + AlF_3 + H_2 + Ti_3C_2 \quad (7)$$

The above-mentioned etching mechanism is still based on utilizing detrimental HF or fluoride solution [98]. To explore a non-hazardous fabrication process, Li et al. [99] proposed a generic strategy to directly etch A-element from the MAX phases by Lewis acids such as $CuCl_2$, $FeCl_2$ and AgCl through a high-temperature molten salt method. During the redox process, the exposed Si atoms in the Ti_3SiC_2 were oxidized into Si^{4+} by cations of Lewis acid. However, the excess Cu^{2+} in the reaction system will react with the exposed Ti atoms on the surface of Ti_3C_2 to form Cu metal particles, which needs to be removed by ammonium persulfate ($(NH_4)_2S_2O_8$, APS) solution (Fig. 4c).

Except the Lewis acidic molten salt method, alkali etching is another feasible method, because Al is amphoteric, soluble in both acids and bases. For example, Xie et al. [100] immersed massive Ti_3AlC_2 in the NaOH solution (1 mol·L^{-1}) and continuously stirred at 80 °C for 100 h to remove the Al atomic layer (Fig. 4d). Finally, multilayered $Ti_3C_2T_x$ was obtained by further removing the un-etched Al element and generating hydroxyl terminal functional groups in 1 mol·L^{-1} H_2SO_4 at 80 °C for 2 h.

Overall, the production of $Ti_3C_2T_x$ MXene multilayer flakes can be achieved by selective etching steps in different ways. However, the multilayer flakes possess small specific surface area and limited amount of available reactive sites, which greatly suppress their potential applications. Therefore, enlarging the interlayer space of $Ti_3C_2T_x$ to gain few-layer ones is necessary. We summarized the delamination methods of $Ti_3C_2T_x$ multilayers in the following section.

3.2 Delamination of $Ti_3C_2T_x$ multilayers

For delamination of $Ti_3C_2T_x$ multilayers, the commonly used strategies of $Ti_3C_2T_x$ are intercalation and ultrasonication methods. Hitherto, the intercalators that have been applied in delamination of $Ti_3C_2T_x$ mainly include some organic reagents such as DMSO [12], tetrabutylammonium hydroxide (TBAOH) [101], tetramethylammonium hydroxide (TMAOH) [13], N-methylpyrrolidone [102] and

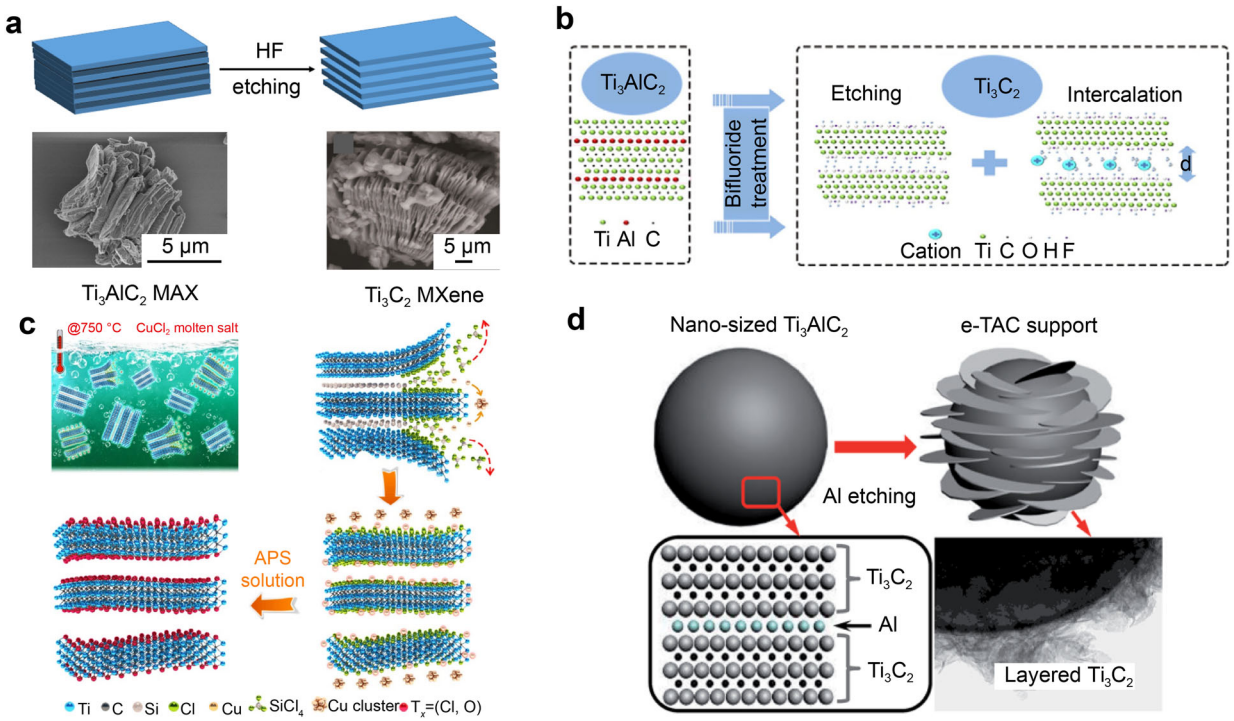

Fig. 4 Synthesis strategies of $Ti_3C_2T_x$ multilayers. **a** Etching Ti_3AlC_2 by HF. Reproduced with permission from Ref. [7]. Copyright 2011, Wiley. **b** Etching Ti_3AlC_2 by XHF_2 bifluoride, where X presents K^+, Na^+, and NH_4^+. Reproduced with permission from Ref. [97]. Copyright 2017, Elsevier. **c** Etching Ti_3SiC_2 by Lewis acids such as $CuCl_2$, $FeCl_2$, and AgCl through a high-temperature molten salt method. Reproduced with permission from Ref. [99]. Copyright 2020, Nature. **d** Etching Ti_3AlC_2 by alkali (NaOH) solution. Reproduced with permission from Ref. [100]. Copyright 2014, The Royal Society of Chemistry

urea [15]. For instance, Mashtalir et al. [12] reported the formation of $Ti_3C_2T_x$-based "paper" by the DMSO intercalation, where the DMSO molecules would get into the separated sheets of $Ti_3C_2T_x$ by sonication, and resulted in increasing lattice spacing of $Ti_3C_2T_x$. Similarly, Chia et al. [101] also took advantage of the large volume of TBAOH molecules to enter the interlayer of $Ti_3C_2T_x$ to promote its delamination. Yang et al. [15] successfully obtained delaminated $Ti_3C_2T_x$ by simultaneous calcination of $Ti_3C_2T_x$ multilayers and urea (Table 1, No. 34). Owing to the abundant functional groups on the surface of $Ti_3C_2T_x$, urea can be tightly adsorbed on its surface, and NH_3 generated by urea during the calcination process can further be employed as a gas template to increase the layer spacing of $Ti_3C_2T_x$ and promote its delamination.

However, the production yield of 2D monolayer $Ti_3C_2T_x$ sheet by delamination is usually unsatisfactory ($\leq$ 20%), which lies in the remaining Ti–Al bonds and potential Ti–Ti bonds between adjacent $Ti_3C_2T_x$ layers after etching. Innovatively, Han et al. [13] used TMAOH as the intercalator, and the yield of monolayered $Ti_3C_2T_x$ achieved the recorded highest value of 74% by a facile hydrothermal-assisted intercalation method (Fig. 5). Compared with DMSO, TMAOH plays better corrosion to Al, and the spatial structure of TMAOH is relatively larger to weaken the interaction between the adjacent $Ti_3C_2T_x$ sheets. Moreover, the formation of $Al(OH)^{4-}$ during the corrosion process will further expand the interlayer space.

To date, the difficulty in layering Ti_3C_2 is generally explained by the strong interaction of potential Ti−Ti bonds between adjacent Ti_3C_2 layers. Meanwhile, since $Ti_3C_2T_x$ is easily oxidized in humid conditions, the layered structure inevitably collapses to a certain extent. When choosing an intercalation agent, one should consider whether it will accelerate the oxidation of $Ti_3C_2T_x$ or not. Therefore, it is still a challenging hot topic for researchers to explore more efficient and environmental-friendly intercalations.

3.3 Synthesis of few-/mono-layer $Ti_3C_2T_x$

Apart from delamination of multilayers, it is feasible to directly prepare uniform and high-quality single-layer $Ti_3C_2T_x$ by adjusting the type and ratio of the etchant and the precursor. Originally, Ghidiu et al. [103] successfully produced single-layer $Ti_3C_2T_x$ flakes from Ti_3AlC_2 via LiF/HCl etching strategy, in which the molar ratio of LiF to Ti_3AlC_2 was 5:1. However, the average diameter of $Ti_3C_2T_x$ flakes obtained after etching was less than 1 μm and had an uneven thickness. In addition, in order to obtain

ultra-thin structure and prevent oxidation, the cumbersome steps of sonicating MXene for 1 h under the protection of argon atmosphere cannot be omitted. Thereafter, Lipatov et al. [16] proposed an optimized method to directly etch Ti_3AlC_2 into high-quality monolayer $Ti_3C_2T_x$ flakes, only through changing the molar ratio of LiF to Ti_3AlC_2 without sonication (Fig. 6). When the molar ratio of LiF to Ti_3AlC_2 increased from 5:1 to 7.5:1, the significantly increased Li^+ amount not only promoted the etching efficiency of Al, but also improved the product quality with a uniform thickness and a smooth surface. In addition, the size of $Ti_3C_2T_x$ flakes was distinctly larger (4–15 μm) than the previous ones (200–500 nm).

In addition to the wet chemical method, direct fabrication of Ti_3C_2 MXene nanosheets can also be achieved by electrochemical methods (Fig. 7). Yang et al. applied Ti_3AlC_2 as the anode in a weak alkaline solution containing ammonium chloride (NH_4Cl) and TMAOH (Fig. 7a) [70]. In this way, Ti_3AlC_2 could be etched in a short time (5 h), and a large number of single or double layered $Ti_3C_2T_x$ with an average size of ca. 2 μm could be obtained. Meanwhile, most of Ti_3C_2 (> 90%) thickness was about 1.2 nm, which is in line with the single layer (Fig. 7b).

3.4 Synthesis of $Ti_3C_2T_x$ quantum dots

Beside of 3D and 2D MXenes, 0D MXenes are also worthy of study due to its potential applications in optical and biological fields. It is because the quantum confinement of small-sized QDs can lead to the expansion of the band gap, and 0D $Ti_3C_2T_x$ has tunable photoluminescence characteristics, which are very suitable for biological imaging and functionalization [20, 104, 105]. Therefore, it is of vital significance to summarize and explore the preparation methods of $Ti_3C_2T_x$ MXene QDs.

The methods of preparing $Ti_3C_2T_x$ MXene QDs mainly include hydro-/solvothermal method [17, 18], ball milling method [19], and micro-explosion method [20] from 3D or 2D MXenes. Most of these strategies follow a similar principle that the bulk structure is cut into smaller quantum particles with the assistance of external force through the defects in the material, which are regarded as the reaction sites. Among the reported strategies, hydro-/solvothermal method was regarded as the most acceptable process for synthesizing $Ti_3C_2T_x$ QDs due to its mild operation conditions. Particularly, Xue et al. [17] prepared $Ti_3C_2T_x$ QDs by a facile hydrothermal route and confirmed that the size and thickness of the obtained $Ti_3C_2T_x$ QDs could be controlled by the hydrothermal temperature and reaction time (Fig. 8a). The appropriate reaction temperature for the synthesis of $Ti_3C_2T_x$ QDs should be 100–180 °C, the pH of the solution was 6–9, and the synthesis time was determined by both temperature and pH value [105]. Analogously, Niu et al. used DMSO, dimethylformamide (DMF), and ethanol as the alternative solvents to synthesize $Ti_3C_2T_x$ QDs by a solvothermal process [18]. Compared with the hydrothermal method, the solvothermal method could accurately control the size and crystallinity of the sample. However, during the solvothermal heating process, carbon QDs were inevitably generated from the utilized organic precursors, which are usually unwanted by-products.

In addition, the ball milling method is also applied to prepare $Ti_3C_2T_x$ QDs, which usually has a high yield. The final morphology and physical properties of the sample depend on the milling speed, milling time, and ball-to-powder weight ratio. For instance, Zhang et al. [19] synthesized $Ti_3C_2T_x$ QDs with the thickness of 2–5 nm using red phosphorus (red-P) and multilayered micro-sized $Ti_3C_2T_x$ as precursors under a high ball milling shear force. The Ti–O–P bonds were formed during the ball milling process, which was the key point to result in the delamination and diminution of $Ti_3C_2T_x$ MXene flakes (Fig. 8b). Beside P, other solid materials such as silicon, sulfur, and carbon could also be added in the ball milling process to induce the formation of Ti–O–X (X = P, C, S, Si) bonds, and it has been found that the stronger the –O–X bond energy is, the smaller the size of the obtained $Ti_3C_2T_x$ QDs is. Generally, this strategy is suitable for the preparation of composite materials (Table 1, No. 33) [19].

In order to explore a more environmental-friendly and efficient method, Li et al. [20] tactfully utilized the great temperature difference between liquid nitrogen and hot deionized water to prepare $Ti_3C_2T_x$ QDs by a self-made micro-explosion method (Fig. 8c). In this strategy, the multilayer $Ti_3C_2T_x$ MXene was firstly flooded with liquid nitrogen, and then hot water was poured in. The water seal formed by hot water and the vaporization of liquid nitrogen promoted the micro-explosion of the layers, thereby destroying the layered structure into $Ti_3C_2T_x$ QDs.

3.5 Synthesis of $Ti_3C_2T_x$-based composites

Owing to the unique structure and surface properties of $Ti_3C_2T_x$, various kinds of materials including metal [106], metallic oxide [107], metal-salt [36], metallic sulfide [37] and organic cellulose [49, 108] have been successfully combined with $Ti_3C_2T_x$ to construct composites for different applications, and it has been widely recognized that the performance of hybrids could be significantly improved with the help of $Ti_3C_2T_x$. This section lists some mainly used preparation strategies for the $Ti_3C_2T_x$-based hybrids in recent years, involving hydro-/solvothermal method, deposition method, self-assembly method, in situ grow method, self-reduction method, and freeze-dried method,

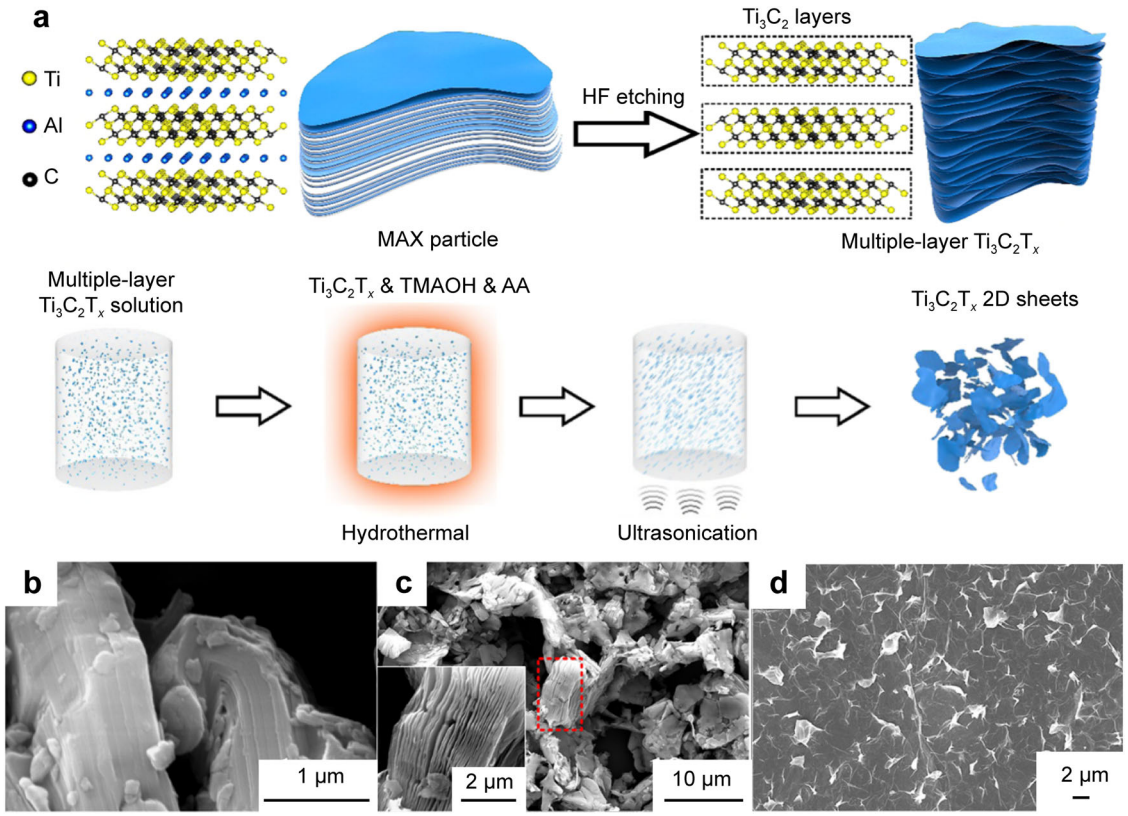

Fig. 5 Delamination of $Ti_3C_2T_x$ multilayers by intercalators. **a** Synthesis process of 2D $Ti_3C_2T_x$ nanosheets by hydrothermal and ultrasonication strategy using tetramethylammonium hydroxide (TMAOH) and ascorbic acid (AA) as intercalators; SEM images of **b** Ti_3AlC_2 precursor, **c** 3D $Ti_3C_2T_x$ multilayers and **d** 2D $Ti_3C_2T_x$ nanosheets. Reproduced with permission from Ref. [13]. Copyright 2019, American Chemical Society

which are summarized in Table 1 for convenience of reference.

3.5.1 Hydro-/solvothermal method

Hydro-/solvothermal method has become the most commonly used strategy for preparing $Ti_3C_2T_x$-based hybrids due to its convenient and simple characteristics. As early as 2017, Ran et al. [37] pioneered the idea of combining CdS with Ti_3C_2 nanoparticles by a hydrothermal strategy, where the Ti_3C_2 nanoparticles served as an efficient co-catalyst for photocatalytic H_2 production (Table 1, No. 6). Since then, articles about employing Ti_3C_2 in the field of photocatalysis have sprung up. For example, Cao et al. [36] prepared a novel 2D/2D $Ti_3C_2T_x/Bi_2WO_6$ heterojunction by in situ growth of Bi_2WO_6 nanosheets on $Ti_3C_2T_x$ ultrathin nanosheets through a hydrothermal method (Table 1, No. 4). Theoretically, when Bi^{3+} and $Ti_3C_2T_x$ nanosheets coexisted in an aqueous solution, Bi^{3+} were readily anchored on the surface of $Ti_3C_2T_x$, because a number of terminal groups (–O or –OH) on the surface of $Ti_3C_2T_x$ resulted in a negative potential. After a simple hydrothermal treatment, with the existence of Na_2WO_6 and cetyltrimethylammonium bromide (CTAB), the intimate contact between $Ti_3C_2T_x$ and Bi_2WO_6 was established. Wang et al. [35] rationally designed $Ti_3C_2T_x$ as a 2D platform to achieve in situ growth of flower-like $Zn_2In_2S_5$ microsphere under an oxygen-free hydrothermal condition (Table 1, No. 3). Jiao and Liu [109] also proposed a facile hydrothermal method that allowed MoS_2 nanosheets grown on $Ti_3C_2T_x$ vertically. Zuo et al. found that under the solvothermal condition, $ZnIn_2S_4$ nanosheets could grow uniformly on the surface of a single-layer Ti_3C_2 to fabricate a heterojunction, which was beneficial to photocatalytic hydrogen production [28].

3.5.2 Deposition method

Through the deposition methods, the chemical substances can be uniformly dispersed on the surface of the receptor objects, and the reaction conditions are not harsh. Thereby, the deposition methods including electrochemical deposition and chemical vapor deposition are also widely applied in the preparation of $Ti_3C_2T_x$-based hybrids. Recently, Yang et al. [38] synthesized a Zn@Ti_3C_2 cathode through a constant-voltage electrochemical deposition technology in

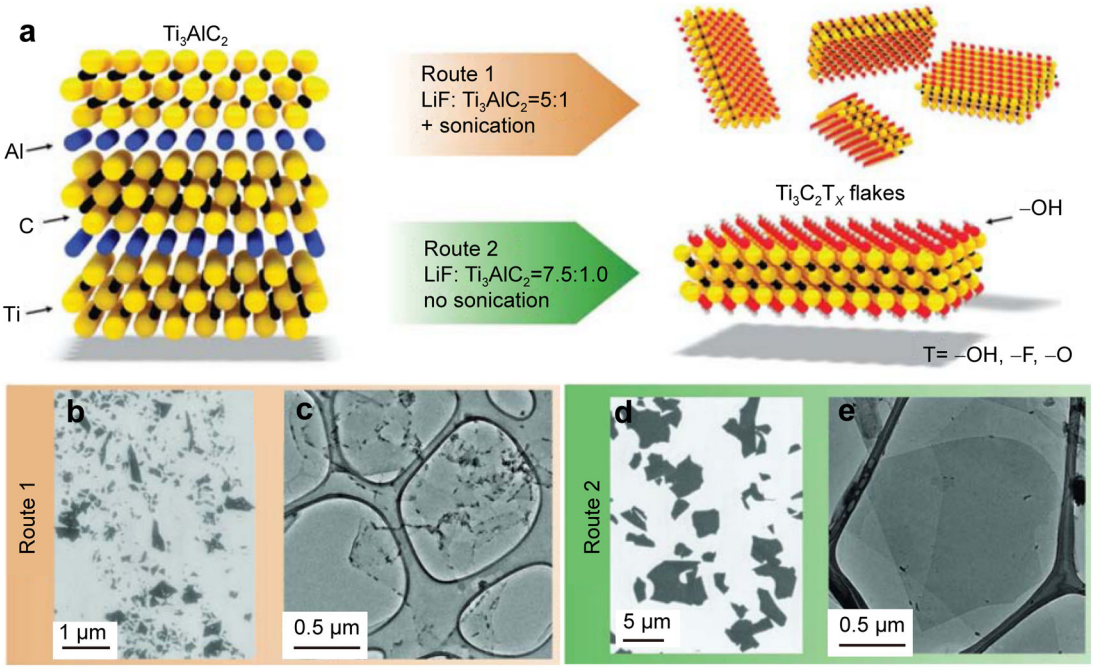

Fig. 6 Synthesis of $Ti_3C_2T_x$ monolayers by chemical etching method. **a** Synthesis process of $Ti_3C_2T_x$ flakes via LiF–HCl etching methods (Route 1: molar ratio of LiF to MAX being 5:1, Route 2: molar ratio of LiF to MAX being 7.5:1.0); **b** SEM and **c** TEM images of obtained $Ti_3C_2T_x$ flakes by Route 1; **d** SEM and **e** TEM images of obtained $Ti_3C_2T_x$ flakes by Route 2. Reproduced with permission from Ref. [16]. Copyright 2016, Wiley

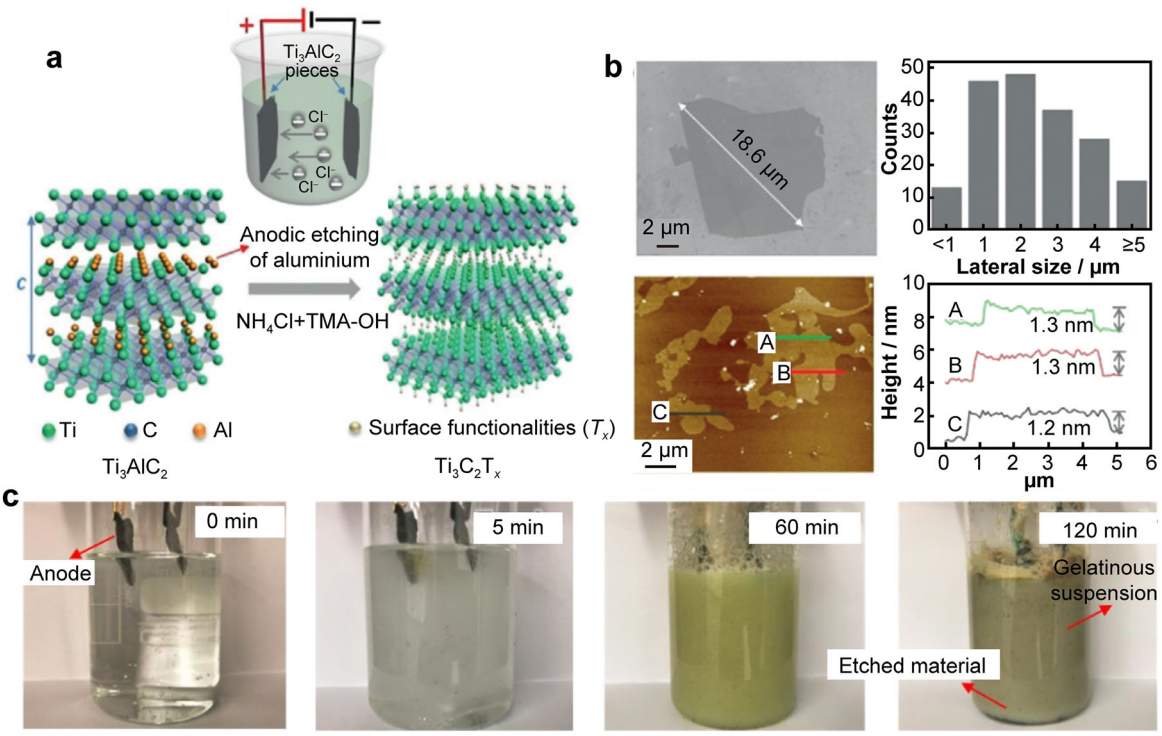

Fig. 7 Synthesis of $Ti_3C_2T_x$ monolayers by electrochemical anodic etching method. **a** Schematic diagram of electrochemical anodic etching process of bulk Ti_3AlC_2 into $Ti_3C_2T_x$ nanosheets. Reproduced with permission from Ref. [70]. Copyright 2018, Wiley. **b** SEM and AFM images of $Ti_3C_2T_x$ nanosheets with corresponding statistical size distribution and relevant height profiles; **c** optical photographs of electrochemical etching process from 0 to 120 min

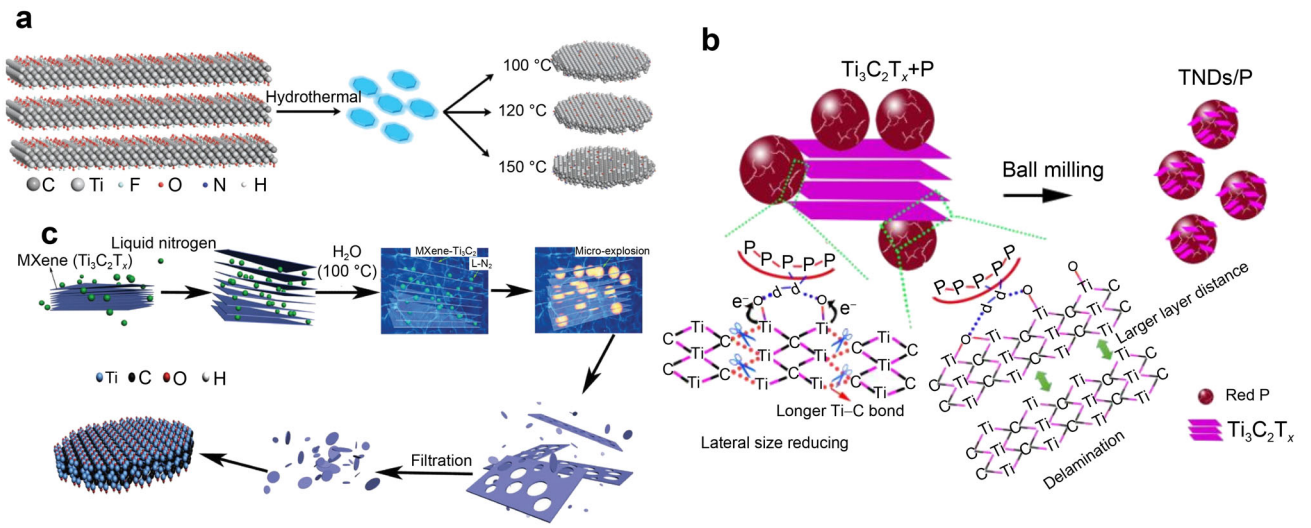

Fig. 8 Synthesis of $Ti_3C_2T_x$ quantum dots. **a** Schematic diagram of effect of hydrothermal temperatures on prepared $Ti_3C_2T_x$ QDs. Reproduced with permission from Ref. [17]. Copyright 2017, Wiley. **b** Formation mechanism of red phosphorus-$Ti_3C_2T_x$ QDs composites via ball milling method. Reproduced with permission from Ref. [19]. Copyright 2018, Wiley. **c** Preparation process of $Ti_3C_2T_x$ QDs by a micro-explosion strategy. Reproduced with permission from Ref. [20]. Copyright 2020, Wiley

a two-electrode system (Table 1, No. 10). Typically, the Ti_3C_2 nanoflakes were used as the work electrode, while a commercial zinc plate was used as the counter electrodes in the reaction system. During the reaction, Zn nanosheets grew vertically on the Ti_3C_2 ultra-thin sheets to form a 3D petal-like structure, which was applied for fabricating biodegradable energy storage systems that deal with increasing amounts of electronic-waste, such as heavy metals. Similarly, Gan et al. [42] prepared a crystalline lithium metal anode with a hair-layer structure by electrochemically depositing lithium on the lithiophilic (LTO)/Ti_3C_2 composite material (Table 1, No. 12). As shown in Fig. 9a, the hair-like LTO grown on the surface of Ti_3C_2 and between the layers could provide a uniformly distributed electric field, which was beneficial to induce the uniform deposition of Li^+. Furthermore, the page-shaped Ti_3C_2 also provided a favorable foundation for Li^+ intercalation. Finally, metal Li anchored smoothly and uniformly on the surface and between layers of Ti_3C_2 to form a mechanically stable structure for lithium anode of the battery. In addition, Li et al. [41] proposed a strategy of fabricating $Ti_3C_2T_x$/CNTs nanocomposite for high-performance electromagnetic wave absorbing material via a facile chemical vapor deposition (Table 1, No. 11). Typically, $Ti_3C_2T_x$ powder was dispersed in an aqueous solution with a certain concentration of nickel nitrate hexahydrate ($Ni(NO_3)_2{\cdot}6H_2O$) as a catalyst, and then freeze-dried. Subsequently, using C_2H_4 as the carbon source, the mixed powder was calcinated at 800 °C, and thus CNTs in situ grew on the surface of $Ti_3C_2T_x$ to form the $Ti_3C_2T_x$/CNTs nanohybrids (Fig. 9b). In this composite, the proper multilaminate structure of $Ti_3C_2T_x$ could effectively prevent the CNTs from stacking.

3.5.3 Self-assembly method

Attributed to the abundant terminal groups (−O, −F, and −OH) on its surface, $Ti_3C_2T_x$ prefers to attract and react with other materials to form strong interfacial contact. To this end, some typical Ti_3C_2-based composites could be rationally fabricated by self-assembly methods. For instance, Xie et al. [43] successfully constructed a 3D porous structured composite of $Ti_3C_2T_x$ and CNTs through an electrostatic self-assembly method (Table 1, No. 13). In detail, $Ti_3C_2T_x$ nanofilms had a hydrophilic surface with a negatively Zeta potential (−63.3 mV), while CNTs were treated by CTAB and thus had a positively Zeta potential (+ 74.8 mV). In the suspension, CNTs were automatically adsorbed on the surface of $Ti_3C_2T_x$ nanofilms through the electrostatic attraction, finally forming a compact structured composite (Fig. 10a). Besides, Guo et al. [46] prepared serine-modified $Ti_3C_2T_x$ by using active sites on serine (such as hydroxyl, amino, and carboxyl) to undergo an esterification reaction with the abundant hydroxyl groups on the surface of $Ti_3C_2T_x$ (Table 1, No. 16). Subsequently, epoxidized natural rubber (ENR) was introduced into the serine-$Ti_3C_2T_x$ in order to overcome the mechanical deformation caused by the inherent rigidity and brittle structure of $Ti_3C_2T_x$. Since the amino group on the serine molecule and the epoxy group on the ENR chain underwent a ring-opening reaction, a serine-grafted epoxy natural rubber (S-ENR) emulsion was formed. Therefore, the

$Ti_3C_2T_x$ nanosheets uniformly dispersed therein were selectively pushed into the gaps of the S-ENR latex microspheres and connected to each other, inducing an ordered 3D conductive network structure (Fig. 10b). Particularly, the natural latex can effectively prevent $Ti_3C_2T_x$ from oxidation during the reaction. Therefore, the mechanical flexibility and sensing performance of the prepared Ti_3C_2/S-ENR sensor can be significantly improved.

Developed rapidly from the 1990s, LBL self-assembly is a simple and multi-functional surface modification method, which can achieve finer control of the material structure, and can also apply uniform coating to the sample. Recently, the driving force of LBL has gradually expanded from electrostatic attraction to hydrogen bonds, and even chemical bonds, which makes it extensively applied in preparing composite materials [110–112]. For instance, An et al. [29] synthesized a Ti_3C_2/PDAC (poly (diallyldimethylammonium chloride)) humidity sensor through a LBL self-assembly method (Table 1, No. 17), using the characteristics that the surface charge of Ti_3C_2 is negative and that of the polymer electrolyte is positive in an aqueous solution with a pH of about 5. Besides, Ma et al. [55] took advantage of the formed hydrogen bond (HB) between the −OH functional group on bacterial celluloses (BCs) and the F− terminal group of $Ti_3C_2T_x$ to synthesize a transparent BCs/MXene composite film, which exhibited an excellent tensile strength and flexibility. In addition to the dominant HB, the density functional theory (DFT) calculations have also been used to testify that a strong chemical bond (Ti–O covalent bond) was generated between $Ti_3C_2T_x$ MXene and BCs.

3.5.4 *In situ grown method*

Typically, $Ti_3C_2T_x$ is extremely unstable in a humid environment and is easily oxidized by water or air. It is the exposed Ti atoms on the surface of $Ti_3C_2T_x$ that are regarded as the nucleation sites to form TiO_2. Inspiring by this feature, Low et al. [50] reported a simple calcination method to in situ convert $Ti_3C_2T_x$ into TiO_2 nanoparticles at 350 °C with a ramping rate of 10 °C·min^{-1}. TiO_2 nanoparticles with uniform size in situ grew on the $Ti_3C_2T_x$ surface, which effectively avoided the particle agglomeration happened in the traditional TiO_2 preparation process (Table 1, No. 22). More significantly, there were a large number of voids between the formed TiO_2 nanoparticles to increase the surface area of the hybrid, which is beneficial to the photocatalytic CO_2 reduction reaction. Similarly, but not the same, Peng et al. [58] directly dispersed $Ti_3C_2T_x$ in a hydrochloric acid solution containing $NaBF_4$ by stirring and ultrasonication, followed by hydrothermal oxidation to easily grow TiO_2 in situ on $Ti_3C_2T_x$ (Table 1, No. 21). In this way, an atomic-level heterojunction was easily formed between TiO_2 and $Ti_3C_2T_x$, which could effectively reduce the charge recombination caused by defects in the bare TiO_2. In addition, Ti_3C_2-IONPs@PEG (iron oxide nanoparticles @amino-[poly (ethylene–glycol)]) compound can also be obtained by an in situ grown method (Table 1, No. 23) [51]. Firstly, by employing ferrous sulfate as the precursor, the IONPs can be grown in situ on the surface of Ti_3C_2 through a redox reaction under alkaline conditions, because the prepared Ti_3C_2 contains negatively charged −O end groups. Afterward, in order to improve the stability of the complex in vivo, PEG was modified on the prepared Ti_3C_2-IONPs by means of electrostatic interactions between Ti_3C_2 and PEG. The constructed composite system can be applied for specific cancer treatment in the tumor microenvironment.

3.5.5 *Self-reduction method*

It is worth noting that during the formation of the single-layer/ultra-thin $Ti_3C_2T_x$ MXene flakes through the acid etching of Al from Ti_3AlC_2, even under mild conditions, some adjacent Ti atoms on the surface of $Ti_3C_2T_x$ will also inevitably be corroded away, which results in the formation of Ti vacancies [113]. These Ti-deficit vacancies are unstable and highly reductive, which can serve as reducing agents for some high-valence metal substances [114]. Taking advantage of this feature, Zhao et al. [25] prepared stable Pt single-atom catalyst over ultra-thin $Ti_{3-x}C_2T_y$ nanofilms with a large number of Ti defects by a synchronous self-reduction stabilization method at room temperature (Fig. 11). In addition, Zou et al. [52] prepared the MXene/Ag composite material by direct self-reduction of $AgNO_3$ in an aqueous solution containing $Ti_3C_2T_x$ (Table 1, No. 24). Similarly, Zhang et al. [115] dispersed poly(vinylpyrrolidone) (PVP) and $Ti_3C_2T_x$ in deionized water at a ratio of 1:1. When the $AgNO_3$ solution is added to the above solution, a large amount of dot-shaped Ag nanocrystalline will be formed, and as the reaction time increases, part of the dot-shaped particles will transform into long strips of precipitate. Finally, urchin-like MXene-based composite will be obtained by regulating the reaction time.

3.5.6 *Freeze-drying method*

Freeze-drying process is based on the sublimation of ice crystals, that is, the moisture in the composites will be directly changed from solid to gas under vacuum conditions. Moreover, the volume of the sample will not change significantly during the freeze-drying process, so its structure can be well preserved. Thereby, the freeze-drying method can be regarded as an efficient solution to prepare

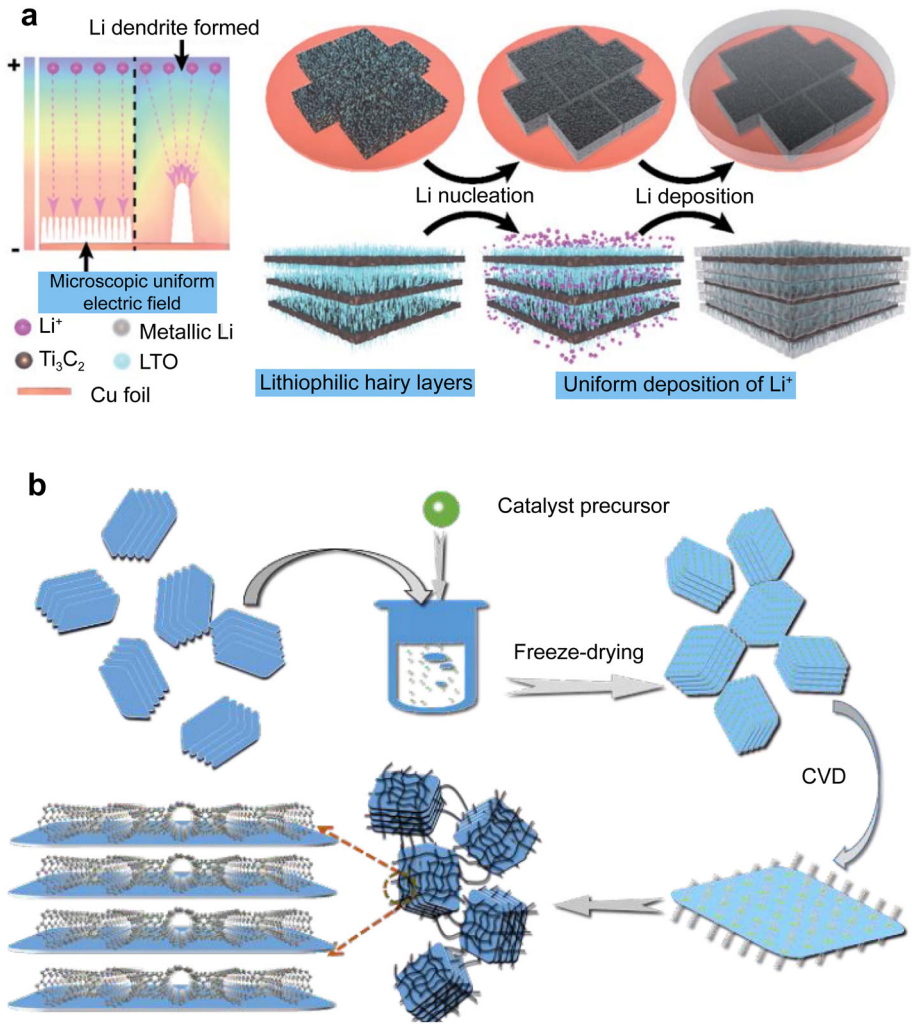

Fig. 9 Preparation of $Ti_3C_2T_x$-based composites by deposition methods. **a** Schematic illustration showing Li deposition behavior on LTO/Ti_3C_2/Cu electrode. Reproduced with permission from Ref. [42]. Copyright 2020, The Royal Society of Chemistry. **b** Synthesis process of $Ti_3C_2T_x$/CNTs hybrids by a chemical vapor deposition method. Reproduced with permission from Ref. [41]. Copyright 2017, The Royal Society of Chemistry

the Ti_3C_2-based compounds with a porous structure and sufficient surface area. Recently, Shi et al. [53] prepared the 3D porous MXene/graphene oxide (MGO) aerogels by a freeze-drying method (Table 1, No. 26). Typically, the prepared Ti_3C_2 nanosheets and GO were uniformly dispersed in the aqueous solution, and sonicated for 10 min in argon atmosphere. Subsequently, the 3D MGO aerogels can be facially obtained after freeze-drying the as-prepared homogeneous solution for 3 days. The highly conductive 3D MGO aerogel can be employed as an anode material for ultra-stable and high-capacity lithium metal batteries.

3.5.7 Other methods

Except the methods as mentioned above, other methods were also reported to prepare $Ti_3C_2T_x$-based composites, such as ultrasound reduction and vacuum filtration. In general, ultrasound will cause the micro-bubbles in the solution to undergo acoustic cavitation and burst, and the rupture of micro-bubbles will generate high temperature. At the same time, water molecules will homogenize at high temperature to produce highly active H· and OH· free radicals. Therefore, Liu et al. [106] slowly added $HAuCl_4$ into the $Ti_3C_2T_x$ suspension under magnetic stirring, and prepared Au/$Ti_3C_2T_x$ composite by sonicating, centrifuging, and drying under the protection of nitrogen, where Au ions were induced to be loaded on $Ti_3C_2T_x$ nanosheets by the reductive H· free radicals.

In addition, filtration method also occupies an important position in the synthesis of Ti_3C_2-based composites due to its simple operation, wide application, and high efficiency. For example, Wang et al. [31] constructed a Ti_3C_2/NMC

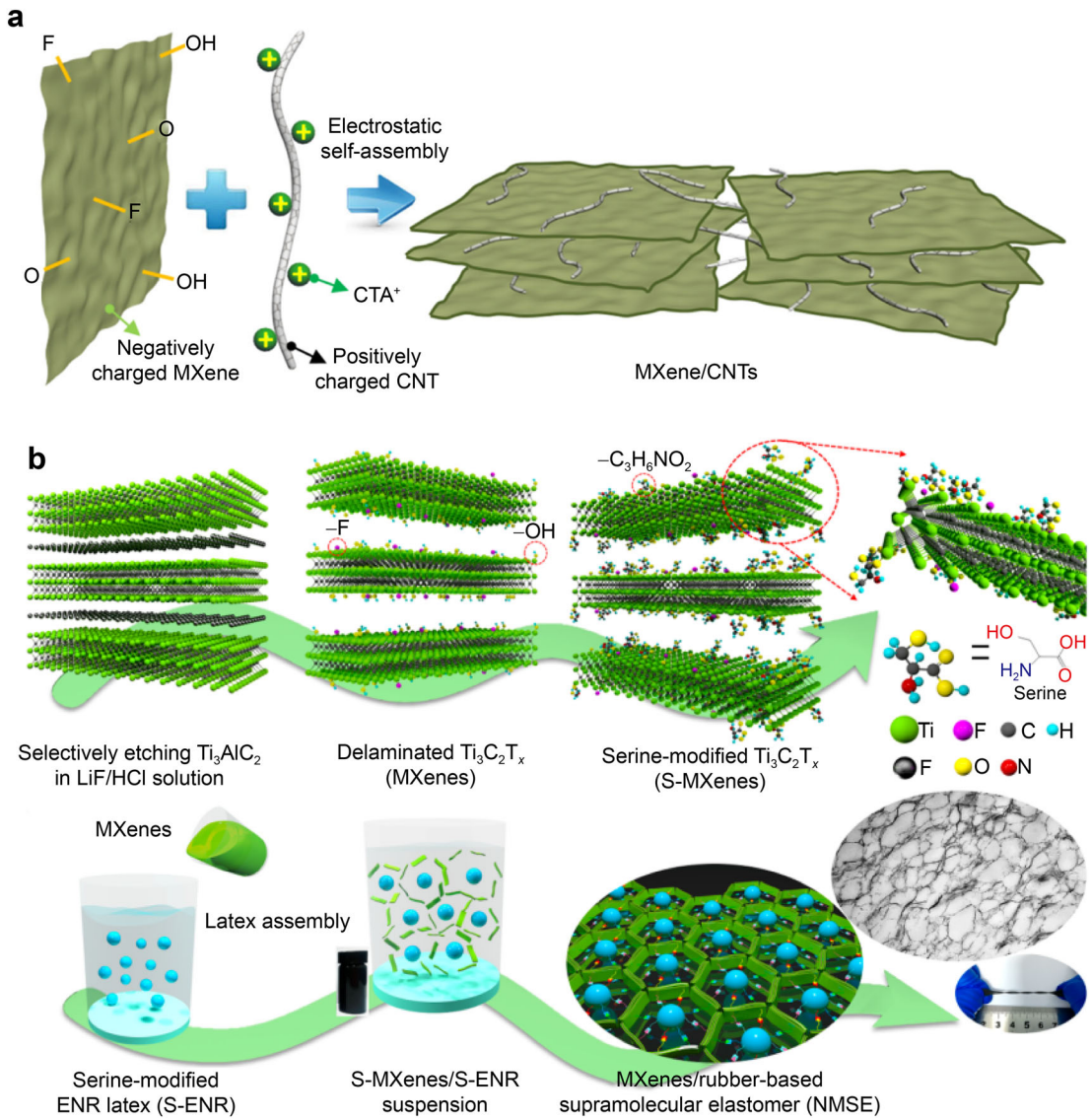

Fig. 10 Preparation of $Ti_3C_2T_x$-based composites by self-assembly methods. **a** Formation diagram of MXene/CNTs via electrostatic self-assembly of negatively charged MXene and positively charged CNTs. Reproduced with permission from Ref. [43]. Copyright 2016, Elsevier. **b** Formation diagram of MXene/rubber-based supramolecular elastomer network via esterification and latex self-assembly process. Reproduced with permission from Ref. [46]. Copyright 2020, American Chemical Society

(natural microcapsule) flexible pressure sensor with assistance of vacuum filtration (Table 1, No. 27). Typically, monolayer Ti_3C_2 aqueous suspension was slowly added into the NMC ethanol suspension, and intensively stirred to form a uniform solution. Then, the Ti_3C_2/NMC biocomposite film was obtained through vacuum filtration with a fine polypropylene fiber membrane.

4 Applications

After introducing the structure, properties, and synthesis of $Ti_3C_2T_x$ MXene, we now turn to their application prospect. Ascribed to their simple preparation process and unique characteristics, the Ti_3C_2-based composite materials have attracted vast attention in the fields of electromagnetic interference, photothermal conversion, biomedicine, energy storage, sensors, photocatalysis, etc. In this section, we will outline the applications of Ti_3C_2 in these fields in detail.

4.1 Electromagnetic wave absorption and shielding

With the development of portable electronic devices and military technology, the exacerbated pollution caused by electromagnetic (EM) wave negatively affected human health and normal electronic communication equipment. In other words, the development of the high-tech intelligent

era has shown a huge demand for protecting electronic instruments and human body from electromagnetic waves.

Recently, Ti_3C_2 MXene has become a hotspot in the microwave absorption (MA) and electromagnetic interference (EMI) fields, because the excellent electrical conductivity and unique layered structure of Ti_3C_2 facilitate some incident electromagnetic waves to be reflected effectively, which improves the conduction loss of the shielding materials to a large extent. Moreover, the presence of terminations on the surface of Ti_3C_2 can cause inherent defects, thus leading to an increase in dipolar polarization, which render Ti_3C_2 a promising candidate for novel MA and EMI absorbing applications. Han et al. [116] designed and fabricated an electromagnetic absorbing material based on $Ti_3C_2T_x$ with an accordion structure. The gained $Ti_3C_2T_x$ films afforded abundant interfaces, which extended the path of electromagnetic wave, and resulted in the attenuation of the electromagnetic wave (Fig. 12a). Moreover, the $Ti_3C_2T_x$ films were annealed and obtained further improved electronic conductivity due to the decrease amount of hydroxyl groups and formation of amorphous carbon on their surface. The reflection coefficient (RC) value of the annealed $Ti_3C_2T_x$ with a loading of 55 wt% on a wax matrix can achieve − 30 dB, and the efficient absorption frequency domain reached up to 2.8 GHz (Fig. 12b). Besides, carbon nanotubes (CNT) were also a good candidate to combine with Ti_3C_2 for electromagnetic interference shielding. For example, Weng et al. [47] fabricated Ti_3C_2/CNT nanocomposite films through a spin spray LBL assembly method (Table 1, No. 18). The obtained thin film shows high conductivity and high electromagnetic shielding efficiency due to the synergistic enhancement effect of Ti_3C_2 and CNT with a layer-by-layer structure. Zhou et al. [57] improved the flexibility and structural stability of Ti_3C_2 nanosheets by repeatedly spraying the composite of Ti_3C_2 and cellulose nanofibers (CNF) on bacterial cellulose (BC) (Table 1, No. 31). Subsequently, CNF/Ti_3C_2/BC films with a compacted layered structure were obtained by hot pressing, which had excellent electrical conductivity and unmatched flexibility. It is worth noting that the CNF/Ti_3C_2/BC composite film was still stable after multiple washings and exhibited good wrinkle resistance, and the shielding effect for EMI was as high as 60 dB. Analogously, Ma et al. [55] took advantage of the chemical bond and hydrogen bond interaction between BC and MXene to synthesize ultra-thin and transparent BCs/Ti_3C_2 films through a simple filtration process (Table 1, No. 29). The composite films exhibited an EMI shielding effectiveness up to ~ 69,455.2 $dB{\cdot}cm^2{\cdot}g^{-1}$.

Overall, the investigation on Ti_3C_2-based hybrids for MA and EMI has obtained a sequence of crucial progress up to date. Nevertheless, compared with the mature graphene-based materials, the MA and EMI properties and mechanisms of Ti_3C_2-based ones are still required to be further researched, which is a long journey for Ti_3C_2 to be practically applied [30].

4.2 Photothermal conversion

As mentioned above, Ti_3C_2 has been testified to be a promising electromagnetic absorbing material. Sunlight, as the optical energy, is also one kind of widespread electromagnetic waves present in our life. Considering that ultimate fate of the absorbed waves is to dissipate in the form of heat within the material demonstrably [30], it can

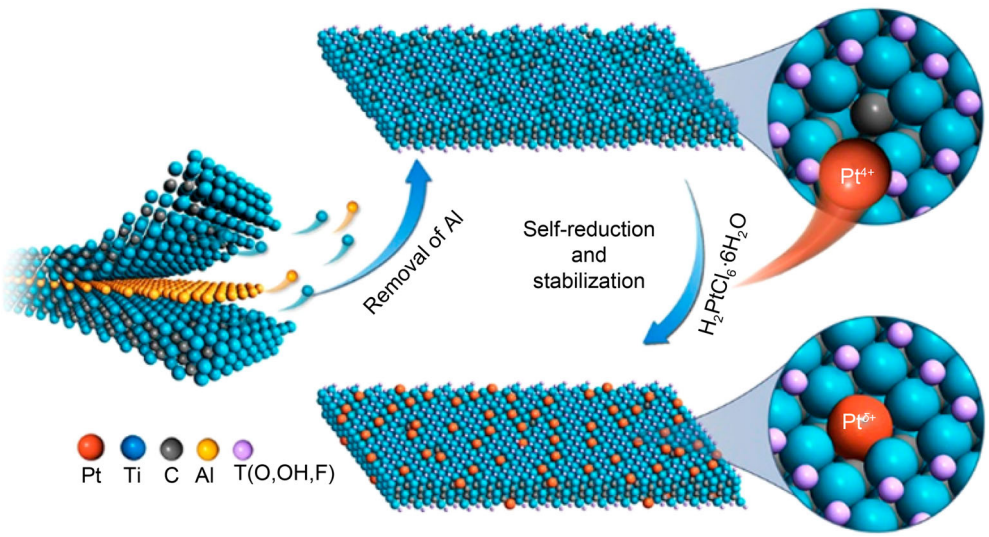

Fig. 11 Simultaneous self-reduction and stabilization process for preparation of $Pt_1/Ti_{3-x}C_2T_y$ catalyst. Reproduced with permission from Ref. [25]. Copyright 2019, American Chemical Society

be reasonably conjectured that Ti_3C_2 can act as a promising light-to-heat conversion material by converting the absorbed microwave into heat energy. Actually, Li et al. [117] fabricated a self-floating Ti_3C_2 film by vacuum filtration with polyvinylidene fluoride (PVDF) membrane as the substrate, and applied it for photothermal water evaporation under sun irradiation (Fig. 12c). Under illumination, the equilibrium temperature of Ti_3C_2-PVDF film achieved a much higher value than that of the pure PVDF membrane (Fig. 12d). In addition, the efficiency of water evaporation was enhanced with increasing Ti_3C_2 ratio. This work has demonstrated that Ti_3C_2 can really be served as a promising photothermal conversion material. Thereafter, Wang et al. [32] successfully constructed a 3D nanoflower–nanosheet structure Cu_3BiS_3/Ti_3C_2 for photothermal seawater desalination (Table 1, No. 5), and the light absorption in the visible-light region exceeded 90%. However, in real life, the propagation of light is multi-angled. In order to improve the ability of the photothermal conversion materials to capture multi-angle light, Yang et al. rationally constructed a Co_3O_4/Ti_3C_2 nanocomposite material as a 3D spherical evaporator (Table 1, No. 9) [40]. The 0D Co_3O_4 was uniformly dispersed on the surface of Ti_3C_2 through its abundant functional groups, and synergistically improved the efficiency of Ti_3C_2 for the absorption and utilization of sunlight. Importantly, the uniformly distributed high-density Co_3O_4 nanoparticles on the surface of Ti_3C_2 effectively blocked the contact of the surface terminal groups with water and oxygen, thereby significantly improving the chemical stability of Ti_3C_2 MXene.

4.3 Biomedical applications

Besides water evaporation and seawater desalination, the photothermal conversion property of Ti_3C_2 was also successfully employed in biomedical field. Liu et al. [118] modified the Ti_3C_2 nanosheets with $Al(OH)_4^-$ to enhance its optical absorption capacity according to the previous report by Xuan et al. [119], then mixed it with doxorubicin (DOX) and hyaluronic acid (HA) to achieve the purpose of killing cancer cells and destroying tumor tissue. Under laser (808 nm, 0.8 $W{\cdot}cm^{-2}$) irradiation, the tumor in mice was completely eliminated without reoccurrence after the injection of the functional Ti_3C_2, which exhibited a high photothermal conversion efficiency of 58.3% in the near-infrared (NIR) range (Fig. 13a). Subsequently, Liang et al. [51] combined photothermal conversion effect of Ti_3C_2 with catalysis reactivity of iron oxide nanoparticles (IONPs) to synthesize a consecutive catalytic system for tumor microenvironment (TME)-specific cancer therapy. The system was fabricated by anchoring natural glucose oxidase (GOD) and superparamagnetic IONPs onto ultrathin Ti_3C_2 nanosheets (Fig. 13b). Glucose was consumed in the presence of GOD to produce hydrogen peroxide and gluconic acid, which were further catalyzed into hydroxyl radicals by IONPs via Fenton reaction. Simultaneously, the NIR light was effectively converted into thermal energy through the light-to-heat ability of Ti_3C_2 nanofilm, which dramatically enhanced the efficiency of catalytic reaction. Finally, the cancer cells were killed by the generated toxic hydroxyl radicals, realizing the high synergistic cancer-therapeutic result.

Interestingly, if the 2D Ti_3C_2 nanosheets are further cut into quantum dots, the unique fluorescence effect and excellent dispersion of $Ti_3C_2T_x$ QDs will provide more suitable services for biomedicine due to the quantum confinement effect. Specifically, Xue et al. [17] have confirmed the development potential of $Ti_3C_2T_x$ QDs as multicolor cell probes in biomedicine and optoelectronic applications by labeling RAW264.7 cells (derived from tumors, induced by Abelson murine leukemia virus). In addition, Li et al. [20] illustrated that Ti^{3+} in the $Ti_3C_2T_x$ QDs could react with H_2O_2 in tumor cells to generate excess toxic hydroxyl radicals, achieving the goal of synergistically killing cancer cells.

Apart from eliminating cancer cells as mentioned above, $Ti_3C_2T_x$ can even serve as a wearable artificial kidney to remove urea, which can provide continuous dialysis for patients with advanced kidney disease (Fig. 13c) [26]. $Ti_3C_2T_x$ has adjustable interlayer spacing and terminal groups, which is advantageous for urea adsorption. The urea adsorption efficiency could reach 99% at room temperature when the content of $Ti_3C_2T_x$ in aqueous solution was 0.83 $g{\cdot}ml^{-1}$. More importantly, the cell viability remained stable even in the $Ti_3C_2T_x$ solution with a high concentration (up to 200 $\mu g{\cdot}ml^{-1}$), which demonstrated the biological harmlessness of $Ti_3C_2T_x$. However, due to the limitations of the 2D structure of $Ti_3C_2T_x$ MXene, it cannot meet the requirements of sustainable drug release, which is of great significance to clinical medicine. Therefore, Xing et al. [49] for the first time synthesized a Ti_3C_2-integrated cellulose hydrogel by using a chemical cross-linking reaction in a low-temperature NaOH−urea−H_2O system (Table 1, No. 32). Replacing terminations on the Ti_3C_2 nanoplatforms by cellulose can make up for the lack of proper biocompatibility of Ti_3C_2. Meanwhile, such cellulose-modified Ti_3C_2 not only improves the carrying capacity of anti-cancer drugs, but the drug release performance of Ti_3C_2 has also been excellently optimized, which can effectively kill tumors and prevent their recurrence.

However, the long-term biosafety of Ti_3C_2 is still a problem to be systematically researched. Further research on controlling the terminal functional groups of $Ti_3C_2T_x$ should be conducted for future biomedical applications. In addition, although $Ti_3C_2T_x$ has excellent dispersibility in

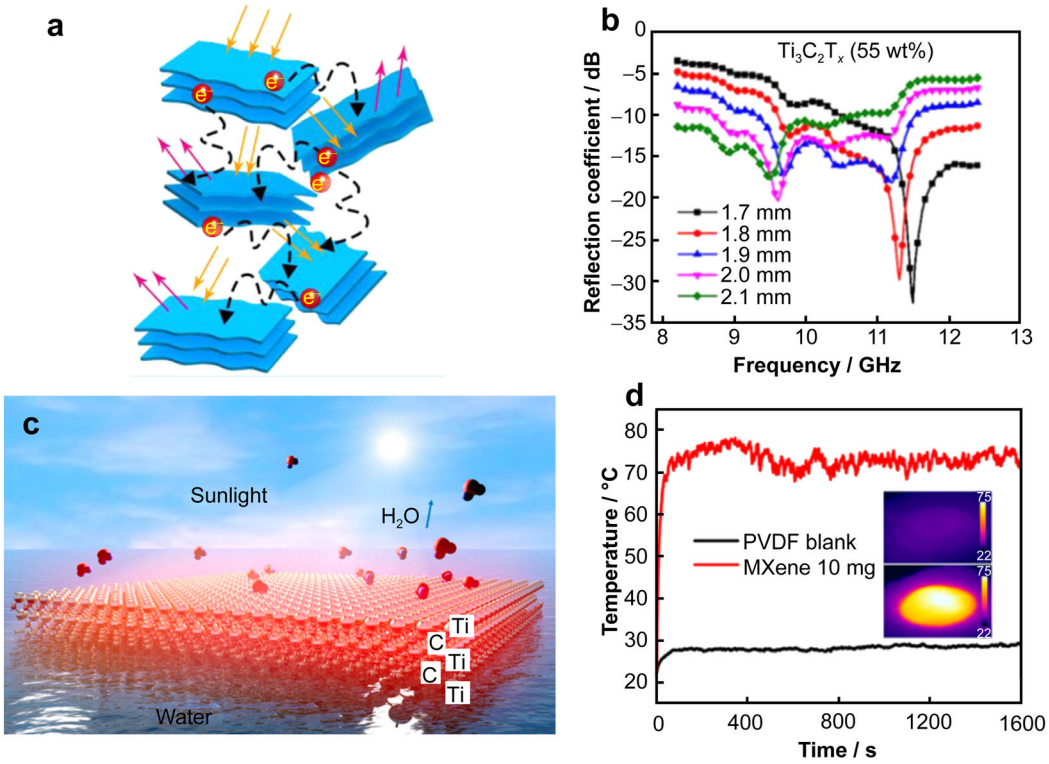

Fig. 12 Applications of Ti_3C_2 in electromagnetic wave absorption and photothermal conversion. **a** Schematic illustration of electromagnetic wave absorption in $Ti_3C_2T_x$ MXenes. **b** Comparison of reflection coefficients of 55 wt% $Ti_3C_2T_x$ on a wax matrix versus frequency with different thicknesses. Reproduced with permission from Ref. [116]. Copyright 2016, American Chemical Society. **c** Schematic diagram of water evaporation over $Ti_3C_2T_x$ MXene via its light-to-heat conversion property; **d** temperature change process of PVDF film and MXene-PVDF film under same condition of illumination and (insets) infrared camera photos of PVDF film and MXene-PVDF film. Reproduced with permission from Ref. [117]. Copyright 2017, American Chemical Society

pure water, its stability in physiological media needs to be ameliorated [120]. Furthermore, in order to realize the convert of $Ti_3C_2T_x$ from laboratory research to medical clinical application, the researching on safe, facile and controllable preparation method of $Ti_3C_2T_x$ with high quality and large quantity is still crucially needed.

4.4 Energy conversion and storage

Batteries and supercapacitors have been a hot research topic for a long time. Nevertheless, the existence issues of low capacity and unstable structure make their practical applications difficult. Fortunately, $Ti_3C_2T_x$-based composite materials emerged and were regarded as a promising electrode candidate for batteries, supercapacitors, and power generators, benefiting from their characteristics of mechanical stability, good electron conductivity, unique multilayered structure, and abundant surface terminations. For example, Shi et al. [53] constructed a stabilized 3D Ti_3C_2 MXene/graphene (MG) framework by anchoring Ti_3C_2 nanosheets on rGO as a dendrite-free lithium (Li)-metal anode (Fig. 14a, Table 1, No. 26). Compared to pure rGO electrodes, the 3D MG effectively suppressed the formation of Li dendrites, because the abundant terminations on the surface of $Ti_3C_2T_x$ were beneficial for the adsorption of Li ions (Fig. 14b). It was noted that the 3D MG electrode maintained an excellent stability and reached a high Coulombic efficiency of ~99% within 2700 h at 5 $mAh{\cdot}cm^{-2}$.

In addition to Li^+ batteries, $Ti_3C_2T_x$ is also a potential anode material for sodium ion (Na^+) batteries. For example, Wang et al. [45] induced the positively charged conductive polyaniline (PANI) into negative-charged $Ti_3C_2T_x$ (Table 1, No. 15). The strong covalent Ti–N bond formed between $Ti_3C_2T_x$ and PANI ensured the stability of the 3D network structure. Moreover, the increased spacing between $Ti_3C_2T_x$ layers and the 3D network structure provided more transmission channels for Na^+, which improved the diffusion kinetics of Na^+ to promote the rate performance and prolong the life of the battery. Homoplastically, Li et al. [121] synthesized MXene functionalized with halogen terminal groups as the cathode of water-based zinc-ion (Zn^{2+}) batteries with extraordinary electrochemical performance (Fig. 14c). In particular, $Ti_3C_2Br_2$ and $Ti_3C_2I_2$ showed distinct electric capacities of 97.6 and 135 $mAh{\cdot}g^{-1}$, respectively (Fig. 14d).

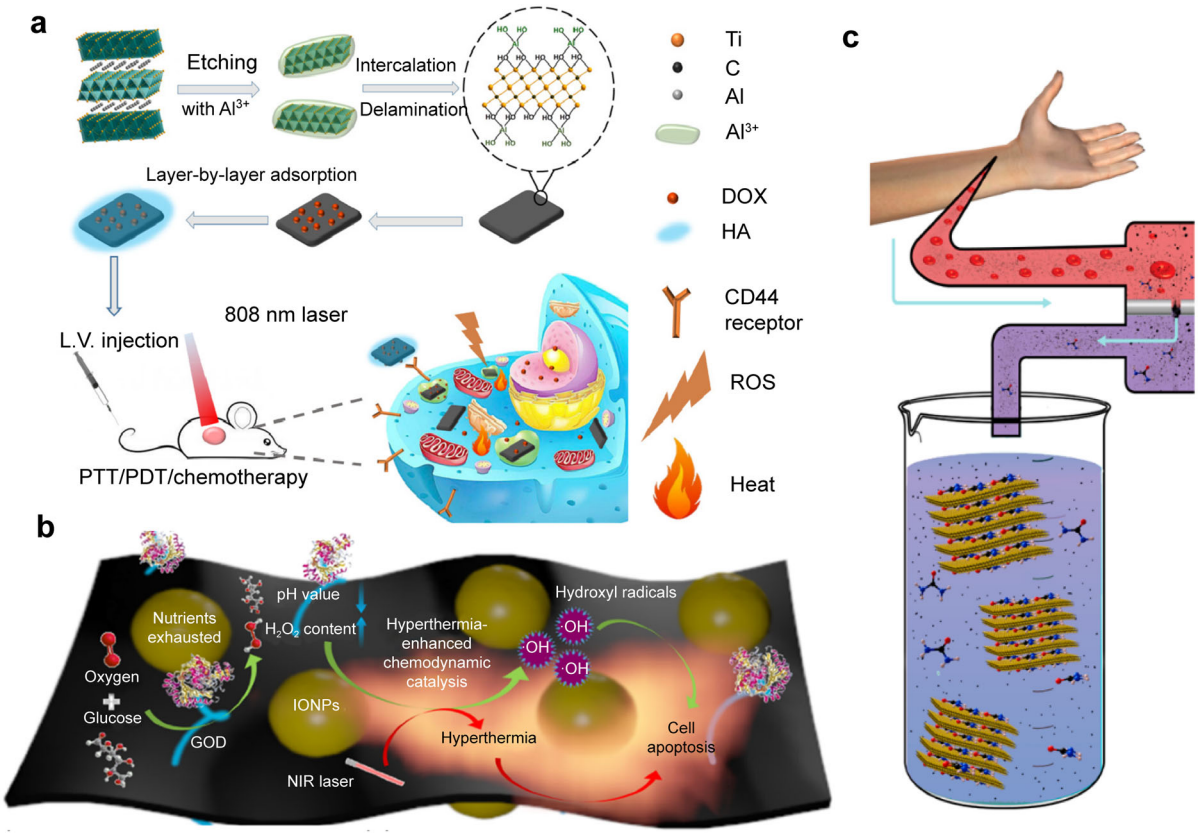

Fig. 13 Applications of Ti_3C_2 MXene in biomedicine. **a** Synthetic process of $Ti_3C_2T_x$-based nanoplatform with a synergistic photothermal effect for tumor chemotherapy, where I.V. injection refers to intravenous injection, and PTT/PDT refers to photothermal/photodynamic therapy. Reproduced with permission from Ref. [118]. Copyright 2017, American Chemical Society. **b** Utilization of glucose oxidase (GOD) and iron oxide nanoparticles (IONPs) modified $Ti_3C_2T_x$ nanoplatforms in synergistic photothermal-catalysis for anti-cancer application under near-infrared light. Reproduced with permission from Ref. [51]. Copyright 2019, American Chemical Society. **c** Simulated process of urea adsorption on 2D $Ti_3C_2T_x$ MXenes dialysis from patient's dialysate. Reproduced with permission from Ref. [26]. Copyright 2018, American Chemical Society

In the prospective energy storage and conversion systems, supercapacitors also occupy an important position, in which mechanical strength is one of the most important test criterions for their practical applications. Chang et al. [54] designed a highly stretchable, bendable, and efficient Ti_3C_2/elastomer electrode by Ag NWs for supercapacitor (Table 1, No. 28). This work indicated that the densely stacked nanosheets in the laminated film are very competitive in electrochemical energy storage due to their high flexibility. However, laminated films usually hinder the diffusion and adsorption of electrolyte ions due to the severe self-stacking of nanosheets. Thereby, Dong et al. reported a molecular ligand-assisted assembly strategy to successfully assemble $Ti_3C_2T_x$ and rGO. After the heat treatment, an ultra-high energy density of 42.1 $Wh{\cdot}L^{-1}$ can be achieved due to the superlattice formed in the MXene–rGO (Table 1, No. 14) [44]. Moreover, the flexible $Ti_3C_2T_x/Nb_2CT_x$ composite membrane was fabricated through alternately stacked by vacuum-assisted filtration (Table 1, No. 30) [56]. After the introduction of $Ti_3C_2T_x$ into Nb_2CT_x, the interlayer spacing was significantly increased compared with that of pure Nb_2CT_x, and the conductivity of the composite membrane was significantly improved. The obtained $Ti_3C_2T_x/Nb_2CT_x$ composite membrane exhibited a mass specific capacitance of 370 $F{\cdot}g^{-1}$ at a scan rate of 2 $mV{\cdot}s^{-1}$, and a capacitance retention rate of 56.1% at 200 $mV{\cdot}s^{-1}$.

4.5 Sensor

As mentioned above, $Ti_3C_2T_x$ has been applied in the wearable electronic devices such as electromagnetic shielding equipment and artificial kidney, all of which are kinds of sensors. Nowadays, most electronic sensors faced with inevitable fractures and low sensitivity in the process of operation, which immensely limits their application in practice. Fortunately, $Ti_3C_2T_x$ can be combined with traditional sensor materials to improve their electrical and/or humidity sensitivity. Besides, the favorable mechanical strength of $Ti_3C_2T_x$ can significantly improve the

mechanical stability and bending resistance of the sensor after introducing into polymer materials. Inspired by the supramolecular interactions of amino acids as the building blocks of a protein, Guo et al. [46] designed a self-healing flexible electric sensor by regularly configuring Ti_3C_2 thin films around the serine-grafted epoxidized natural rubber (S-ENR) latex to form a 3D conductive network via hydrogen bonding interaction (Table 1, No. 16). When people make various expressions such as smiling, astonishing, and frowning, the facial muscle states are totally different, which leads to the discrepancies of electrical signals (Fig. 15a). The obtained flexible electric sensor could detect those different tiny electrical signals due to its high sensitivity and precision rate. Analogously, inspired by sensing mechanisms of human skin, Wang et al. [31] constructed a Ti_3C_2/natural microcapsule (NMC) biocomposite membranes to achieve the human—machine interactions (Fig. 15b, Table 1, No. 27). The stable and flexible sensing device has realized voice recognition via detecting and distinguishing different signals from human motion and pulses. Up to now, the developments of Ti_3C_2-based functional composites in sensor applications are still in initial stage. However, the combination of Ti_3C_2 has effectively overcome the disadvantages of traditional sensors, such as inevitable buckling and fracturing in their working process, which paved the broad road.

4.6 Photocatalysis

Photocatalytic technology based on semiconductor materials is regarded as an effective measure to remit the issues of energy crisis and environmental pollution [122]. Up to now, the semiconductors including TiO_2, CdS, $ZnIn_2S_4$, and g-C_3N_4 have been widely studied due to their suitable band structure and controllable morphologies [123–127]. However, the traditional single semiconductor catalyst has poor light utilization efficiency and low carrier separation efficiency. Supporting co-catalysts and building heterojunctions are common strategies to solve the above problems. In view of this, the merits of $Ti_3C_2T_x$ including appropriate energy band structure, excellent electron conductivity, popular price, and hydrophilic surface endowed it with incredible potential in the photocatalysis application fields, such as hydrogen (H_2) production from water splitting, CO_2 reduction, nitrogen (N_2) fixation, and pollutant degradation.

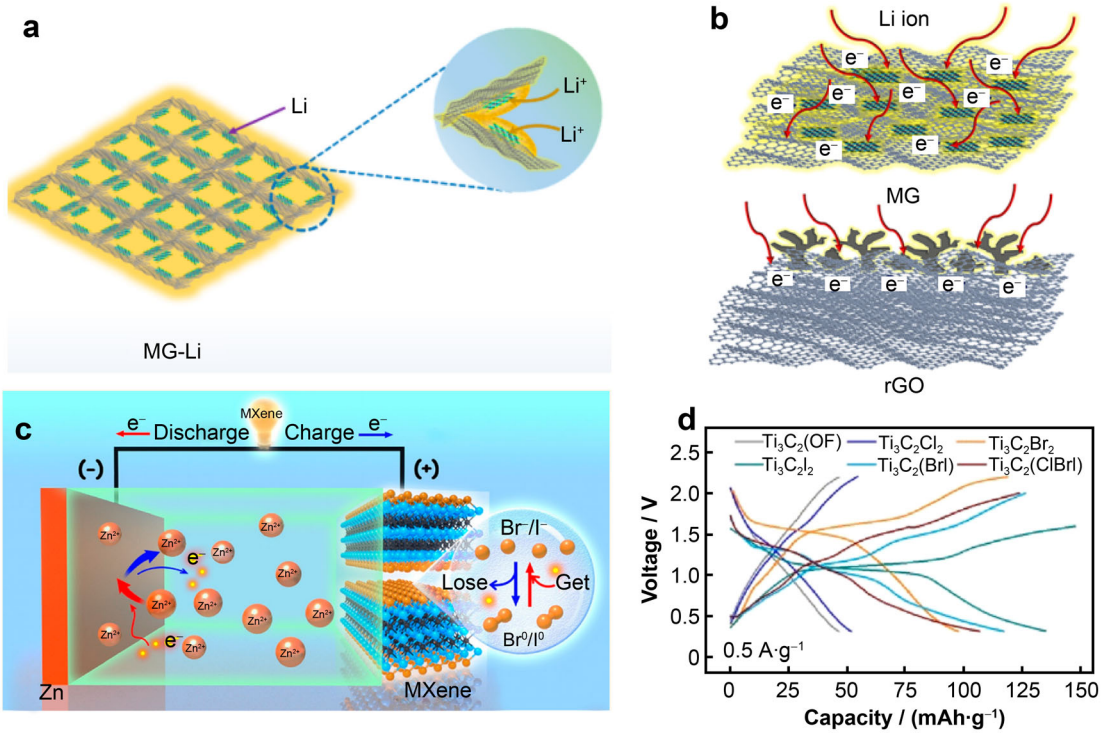

Fig. 14 Applications of Ti_3C_2 MXene in energy conversion and storage. Schematic illustration of **a** Ti_3C_2 MG anode and **b** processes of Li^+ plating and striping into MG and pure rGO electrodes, respectively. Reproduced with permission from Ref. [53]. Copyright 2019, American Chemical Society. **c** Schematic diagram of charging and discharging process of Ti_3C_2 MXene as cathode in an aqueous zinc-ion battery; **d** typical galvanostatic charge−discharge curves of $Ti_3C_2T_x$ with different functional groups at current density of 0.5 $A{\cdot}g^{-1}$. Reproduced with permission from Ref. [121]. Copyright 2021, American Chemical Society

4.6.1 Hydrogen production

For H_2 production, Ran et al. [37] for the first time utilized theoretical calculations to systematically evaluate the ability of $Ti_3C_2T_x$ as a co-catalyst in the process of photocatalytic H_2 production from water splitting. Generally, the entire H_2 evolution reaction (HER) pathway can be summarized into three processes: (I) initial state of $H^+ + e^-$, (II) intermediate adsorption of H*, and (III) final production of H_2 [128]. Therein, the Gibbs free energy ($|\Delta G_{H^*}|$) of the second stage is the key factor to evaluate the performance of the catalyst, the most theoretically suitable value of which is zero for H_2 evolution [129]. Ran et al. [37] constructed a 4 × 4 × 1 O-terminated $Ti_3C_2T_x$ supercell ($Ti_3C_2O_x$) as shown in Fig. 16a, and the Gibbs free energies of the $Ti_3C_2O_x$ with different hydrogen atomic (H*) coverage on the surface were calculated based on the DFT method. As shown in Fig. 16b, the $|\Delta G_{H^*}|$ value for $Ti_3C_2O_x$ with an H* coverage of $\theta = 1/2$ was inspiringly 0.00283 eV, extremely close to zero, which indicated that it is beneficial to promote the H_2 production efficiency of semiconductors from the thermodynamic point of view. Therefore, they accordingly modified CdS with Ti_3C_2 QDs for enhanced visible-light photocatalytic H_2 production, which achieved an extremely high H_2 production rate of 14,342 $mmol \cdot h^{-1} \cdot g^{-1}$ with the corresponding apparent quantum efficiency of 40.1% at 420 nm (Table 1, No. 6). According to the relationship between the band structures of CdS and Ti_3C_2, the charge transfer mechanism was following the schemes in Fig. 16c, d. It was also found that the photocatalytic activity of the composite was enhanced with the decreasing atomic ratio of F to O on the $Ti_3C_2T_x$ surface (Fig. 16e).

Homoplastically, taking advantage of suitable Fermi level position, a large number of hydrophilic functional groups, and good electronic conductivity, Ti_3C_2 was also verified to be an effective co-catalyst of the $ZnIn_2S_5$ [35] and $ZnIn_2S_4$ [28] photocatalysts for H_2 production (Table 1, Nos. 3 and 7). Furthermore, Su et al. [107] experimentally confirmed that monolayer Ti_3C_2 performed better in improving the photocatalytic H_2 production activity of TiO_2 than multilayer Ti_3C_2, because the monolayer one with abundant hydrophilic functional groups on its surface tended to adsorb water molecule and simultaneously provided more active sites for H_2 production. More importantly, there are abundant Ti vacancy defects with strong reducibility on the monolayer or ultrathin $Ti_3C_2T_x$ nanosheets prepared by the wet etching method, which can realize the reduction of high-valent metal salts without adding extra reducing agents and energy input [130]. Based on this feature, Li et al. [24] reported a simple reduction and self-assembly strategy to construct a ternary CdS@Au/MXene composite photocatalyst (Table 1, No. 8), which exhibited a photocatalytic H_2 production rate of 5371 $\mu mol \cdot g^{-1} \cdot h^{-1}$ under visible-light irradiation, nearly 27 times higher than that of pure CdS.

4.6.2 CO_2 conversion

Similar to the role played in photocatalytic H_2 production, Ti_3C_2 also can serve as a co-catalyst to enhance the performance of semiconductors for photocatalytic CO_2 reduction. For example, Cao et al. [36] demonstrated that the yields of CH_4 and CH_3OH produced from CO_2 reduction on the Ti_3C_2/Bi_2WO_6 nanohybrid (Table 1, No. 4) were, respectively, 4 and 6 times higher than those produced on pure Bi_2WO_6 nanofilms (Fig. 17a). The intimate contact between Ti_3C_2 nanosheets and Bi_2WO_6 ultrathin nanofilms was the key factor to improve the separation and transfer efficiency of photogenerated charge carriers, which greatly enhanced the performance of photocatalytic CO_2 reduction. Since the Fermi level of Ti_3C_2 with –O termination was more positive than the conduction band edge of Bi_2WO_6, the photoinduced electrons can transfer from Bi_2WO_6 to Ti_3C_2 (Fig. 17b). Similarly, the Ti_3C_2/g-C_3N_4 composite prepared by Yang et al. [15] also facilitated the electron transferring from g-C_3N_4 to Ti_3C_2, which was beneficial to the improvement of the CO_2 reduction performance, and the highest CO yield reached up to 5.19 $\mu mol \cdot h^{-1} \cdot g^{-1}$.

In addition, CO_2 can also be converted into other green energy sources through photocatalytic reactions with the assistance of Ti_3C_2. Zhao et al. [25] used Ti_3C_2 nanosheets rich in Ti vacancies to construct a single-atom catalyst (SAC) $Pt_1/Ti_{3-x}C_2T_y$ through a self-reduction process at room temperature (Table 1, No. 25). Owing to the high reduction ability of the Ti vacancies, single-atom Pt can be successfully stabilized on the Ti defects through strong metal–carbon bonds. Compared with traditional single-atom catalysts, the utilization of Ti_3C_2 nanosheets as supporting substrates can effectively overcome the shortcomings of reduced catalytic efficiency caused by the aggregation of dispersed single atoms. Meanwhile, the inherent reducing ability of defective Ti_3C_2 can omit the conditions of reducing atmosphere (H_2 or Ar) required in the traditional preparation process of SAC. In this way, CO_2 can contact the evenly distributed Pt atoms on the nanosheets more efficiently, so that the functionalization efficiency of CO_2 can be effectively improved when amines and silanes are present in the system.

It has to be mentioned that Ti_3C_2 MXene can also construct composite catalysts with other semiconductors in the shape of QDs to optimize the capabilities of CO_2 reduction and conversion. Compared with 2D ultra-thin nanosheets, 0D QDs can be more uniformly dispersed in

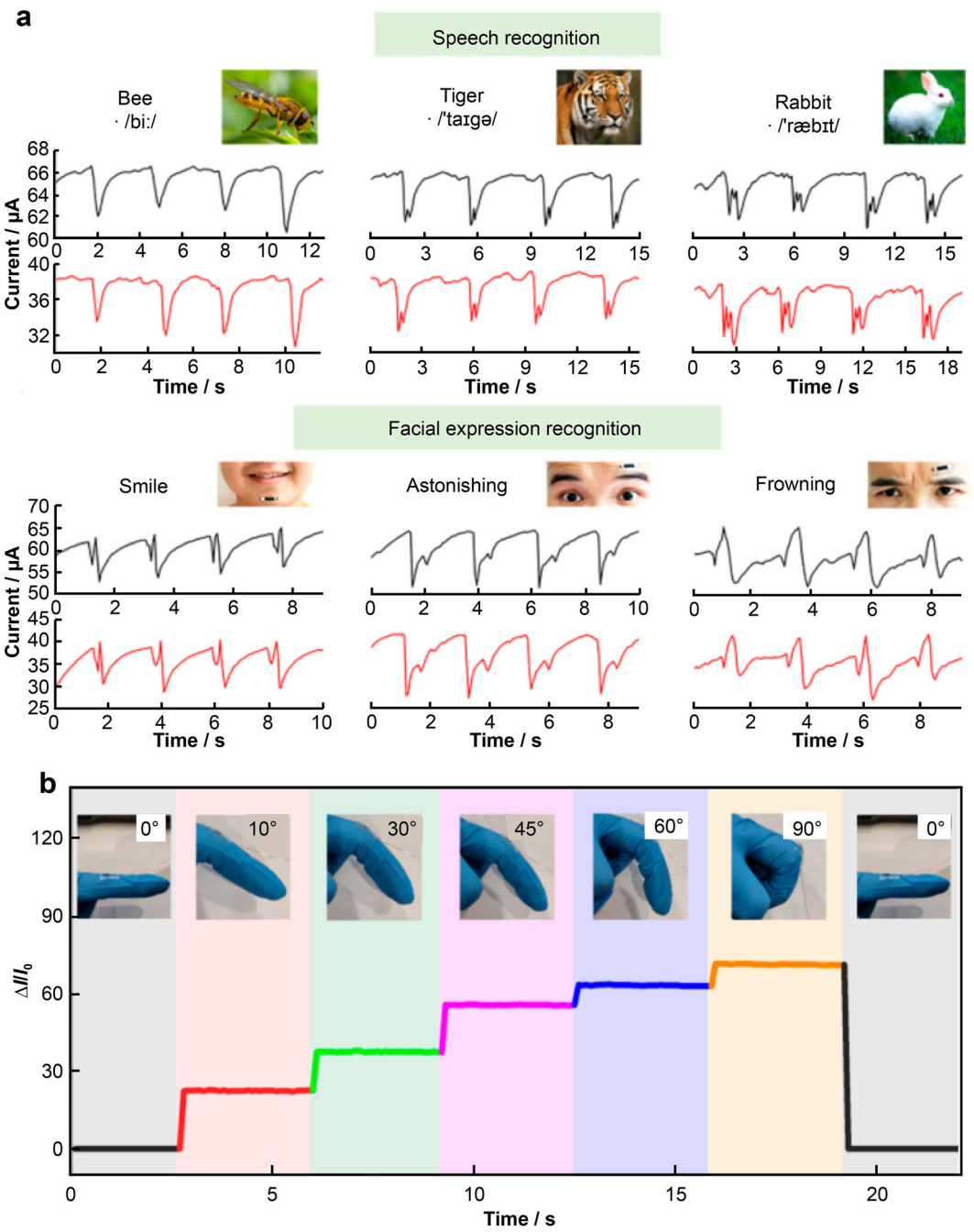

Fig. 15 Applications of Ti_3C_2 MXene in sensors. **a** Respond of Ti_3C_2-based sensors to currents generated by different voices and facial expressions. Reproduced with permission from Ref. [46]. Copyright 2020, American Chemical Society. **b** Relative current change of Ti_3C_2/NMC (natural microcapsule) flexible sensor when finger was bent at different angles. Reproduced with permission from Ref. [31]. Copyright 2019, American Chemical Society

the liquid and have abundant active edge sites. Reported by Zeng et al. [39], the negatively charged Cu_2O NWs/Cu modified with poly(sodium 4-styrenesulfonate) (PSS) and the positively charged $Ti_3C_2T_x$ QDs modified with polyethylenimine (PEI) were combined to fabricate $Ti_3C_2T_x$ QDs/Cu_2O NWs/Cu composites through electrostatic self-assembly strategy (Table 1, No. 19). Under calcination in argon atmosphere, PSS and PEI molecules can be completely removed so that $Ti_3C_2T_x$ QDs and Cu_2O NWs were closely contacted. The efficient conversion of CO_2 to methanol by ternary $Ti_3C_2T_x$ QDs/Cu_2O NWs/Cu was 8.25 times higher than that of the pure

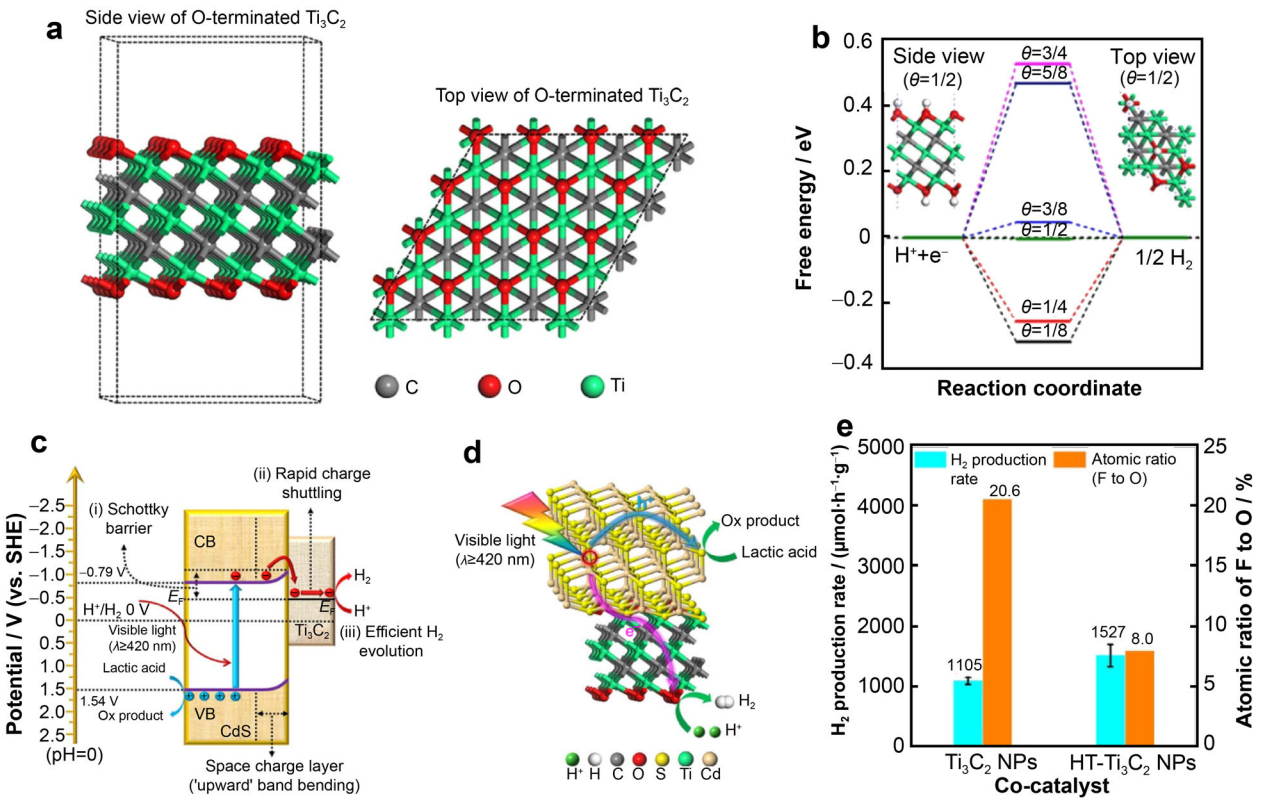

Fig. 16 DFT calculation results of O-terminated $Ti_3C_2T_x$. **a** Side and top views of structure model for a 4 × 4 × 1 O-terminated $Ti_3C_2T_x$ supercell; **b** calculated ΔG_{H^*} diagram of HER at equilibrium potential (U = 0 V) on surface of a 2 × 2 × 1 $Ti_3C_2O_x$ supercell at different H* coverage (1/8, 1/4, 3/8, 1/2, 5/8 and 3/4) conditions (inset: side and top views of a 2 × 2 × 1 $Ti_3C_2O_x$ supercell at 1/2 H* coverage); **c** energy band structures of CdS and Ti_3C_2, and charge transfer mechanism of CdS/Ti_3C_2 system under visible-light irradiation; **d** charge transfer route over interface of CdS/Ti_3C_2 system under visible-light illumination; **e** influence of Ti_3C_2's surface F to O atomic ratio on photocatalytic activity. Reproduced with permission from Ref. [37]. Copyright 2017, Nature

Cu_2O NWs/Cu. Similarly, $Ti_3C_2T_x$ QDs were also employed to improve the photocatalytic CO_2 reduction ability of TiO_2/C_3N_4 (Table 1, No. 20) [48]. The conversion rates of CO and CH_4 were 3 and 8 times higher than those of pure TiO_2 and C_3N_4, respectively.

4.6.3 Nitrogen photofixation

For practical applications in industries, the ultimate goal of N_2 fixation is to realize its conversion to ammonia (NH_3), which is of great significance for the modern agricultural production, because NH_3 is the main source of nitrogen element in artificial fertilizers. Generally, the difficulty for the synthesis of NH_3 from N_2 lies in the strong N≡N triple bond energy (945 kJ·mol^{-1}) of N_2 [126], and it is indispensable to accumulate multiple electrons on the surface of the photocatalyst because N_2 reduction is a multi-charge transfer process.

Currently, the outstanding conductivity of $Ti_3C_2T_x$ lays the foundation for its excellent performance in the N_2 reduction reactions. Besides, the exposed Ti vacancies on the surface and edges of the $Ti_3C_2T_x$ and the large specific surface area could provide abundant active sites for the N_2 adsorption and activation. In 2019, Qin et al. [131] reported that 0D/2D $AgInS_2/Ti_3C_2$ Z-scheme heterojunction prepared by a hydrothermal method was applicable in solar photocatalytic N_2 fixation. The photocatalytic N_2 fixation rate under visible light (< 400 nm) could reach 38.8 μmol·g^{-1}·h^{-1}. The Z-scheme heterostructure formed between Ti_3C_2 and $AgInS_2$ accelerated the accumulation of multiple electrons on the surface of Ti_3C_2, thereby achieving efficient charge separation and migration (Fig. 18a). In addition, this work used DFT simulations to investigate the adsorption and activation behavior of N_2 on the Ti_3C_2 (001) surface. The result showed that the maximum adsorption energy of NH_3 on Ti_3C_2 was −5.20 eV, and the length of the N≡N bond increased from 0.1098 to 0.1334 nm, indicating a weakening of the N≡N bond. The above results confirmed that N_2 molecules tended to be activated with the aid of Ti_3C_2 (Fig. 18b).

Based on the above research, Liao et al. [132] compounded Ti_3C_2 with P25 TiO_2 and measured the performance of photocatalytic NH_3 synthesis. Under full-spectrum light irradiation, the NH_3 generation rate of the

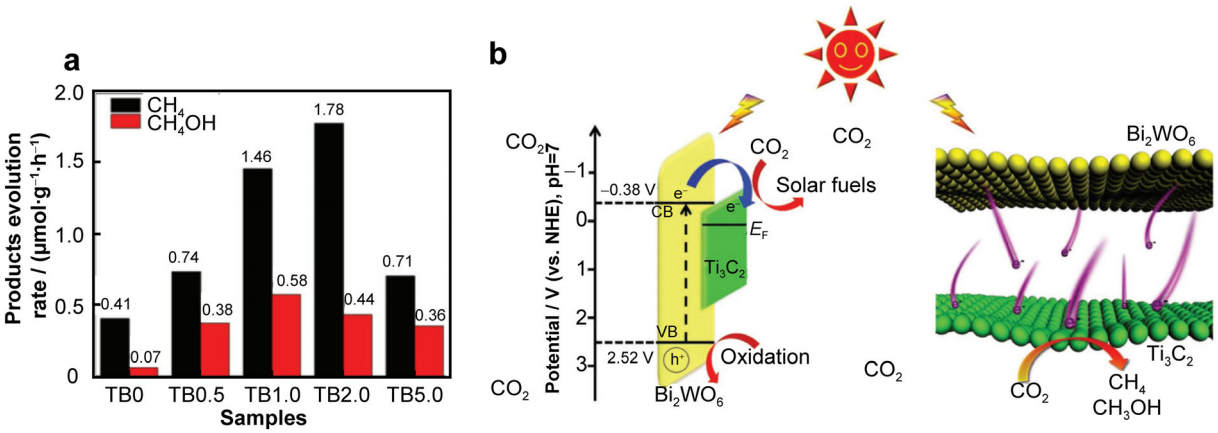

Fig. 17 Application of Ti_3C_2 MXene in CO_2 conversion. **a** Photocatalytic activity of pure Bi_2WO_6 and Ti_3C_2/Bi_2WO_6 (TB*x*) nanohybrids with different Ti_3C_2 contents; **b** energy level diagram of Bi_2WO_6 and Ti_3C_2 and photoinduced electron transfer process at interface of Ti_3C_2/Bi_2WO_6 hybrids. Reproduced with permission from Ref. [36]. Copyright 2018, Wiley

optimized Ti_3C_2/P25 sample was 5 times higher than that of bare P25. Similarly, the DFT calculations also confirmed that Ti_3C_2 can significantly improve the efficiency of N_2 chemical adsorption and activation. Furthermore, Sun et al. [133] developed 1D/2D CdS nanorod@Ti_3C_2 MXene composites for photocatalytic NH_3 synthesis with the N_2 fixation rate of 293.06 $\mu mol \cdot g^{-1} \cdot h^{-1}$.

Herein, N_2 photofixation on MXene materials is still in its infancy. More in-depth research is needed to reveal the N_2 adsorption model on MXene, as well as the effect and mechanism of MXene in the reaction process of photonitrogen fixation and ammonia synthesis.

4.6.4 Pollutant degradation

$Ti_3C_2T_x$ also plays a central role in photocatalytic pollutant cleanup. For example, Peng et al. [58] synthesized (001) $TiO_2/Ti_3C_2T_x$ composites by a facile hydrothermal process, which exhibited significantly enhanced photocatalytic degradation efficiency of methyl orange (MO) than bare TiO_2. As illustrated in Fig. 19a–c, on the basis of DFT calculation results, the work function values of the $Ti_3C_2T_x$ with −OH terminal groups and TiO_2 with (001) surface exposed were calculated to be 1.800 and 4.924 eV, respectively. Since the "work function" of a material is defined as the difference between its Fermi level (E_f) and the vacuum level (E_{vac}), it can be inferred that the E_f of the OH-terminated $Ti_3C_2T_x$ is higher than that of the (001) TiO_2. Therefore, after they are tightly contacted, a new balanced Fermi level would be formed between their original ones. Meanwhile, the energy band edge of (001) TiO_2 will bend downward to form a Schottky heterojunction with $Ti_3C_2(OH)_x$, which will trap the holes from TiO_2 and thus largely reduce the recombination of charge carriers. Under this circumstance, the Ti_3C_2 was regarded to be a reservoir of photogenerated holes. Similar mechanism was also applied to explain the enhanced photocatalytic performance of (111) $TiO_2/Ti_3C_2T_x$ and Cu/TiO_2@$Ti_3C_2T_x$ composites (Table 1, Nos. 1 and 2) [33, 34].

However, there are some arguments to the contrary. For example, Low et al. [50] reported that the Ti_3C_2 acted as the trap of electrons in the TiO_2/Ti_3C_2 composite for highly efficient photocatalytic CO_2 reduction. The difference might lie in the chosen model structures for the DFT calculations. As shown in Fig. 19d–f, Ti_3C_2 with no terminal groups and TiO_2 with (101) surface exposed were chosen to be the calculating object, whose work functions were 4.46 and 4.25 eV, respectively. Therefore, after their contact, the energy band edge of (101) TiO_2 will bend upward to form a Schottky heterojunction with Ti_3C_2. In this case, the Ti_3C_2 served as a reservoir of photogenerated electrons from TiO_2 instead.

Therefore, in order to determine the actual role of Ti_3C_2 in the composite photocatalyst by DFT calculations, it is necessary to build that structural model as close to reality as possible, paying particular attention on the terminal groups on Ti_3C_2 and surface atomic configuration of TiO_2. Different calculation methods may also influence the final conclusion on the proposed charge transfer mechanism.

Overall, in the field of photocatalysis, (1) $Ti_3C_2T_x$ with different terminations could serve as electrons or holes acceptor to play as an effective co-catalyst in various photocatalysis systems. (2) Owing to appropriate Fermi level, Ti_3C_2 could couple with various semiconductor materials to establish Schottky junction, which could suppress recombination of electron or hole. (3) The intrinsic Ti vacancies in $Ti_3C_2T_x$ could act as reduction sites for cations to form single-atom catalyst and binary/ternary composite catalyst. However, the proposed mechanisms of $Ti_3C_2T_x$ as the co-catalyst in the previous literatures were

actually inadequate and worthy further consideration. Meanwhile, the development of new strategies to prepare $Ti_3C_2T_x$ with different end groups to regulate its Gibbs free energy and energy band structure is still a challenge worthy of breakthrough in the field of photocatalysis.

5 Summary and future opportunities

To summarize, considerable achievements and excellent progress have been made in the $Ti_3C_2T_x$ material, which has been recognized as one of the most thoroughly studied materials in the MXene family due to its various excellent properties, such as flexible structures, good conductivity, hydrophilicity, and mechanical stability. Consequently, researchers have taken much effort to combine the advantages of $Ti_3C_2T_x$ with traditional inorganic, organic, and polymer materials to overcome the development obstacles in the conventional functional materials. So far, the explored preparation methods of the $Ti_3C_2T_x$-based composites include hydro-/solvothermal method, deposition, self-assembly, in situ growing, freeze-drying method, and other strategies. Followed by, the obtained composite has been successfully applied to energy storage, electromagnetic interference, photothermal conversion, biomedicine, sensors, photocatalysis, and other fields, and has made considerable progress. By summarizing the examples mentioned in this review, it can be seen that the discovered properties of $Ti_3C_2T_x$ have been successfully applied in corresponding fields, following some certain disciplines.

(1) A large number of terminal groups such as –O, –F, and –OH on the surface of $Ti_3C_2T_x$ render it a negative surface, which is particularly attractive to positively charged ions or ligands, providing more active sites and possibilities for the reactions in need.

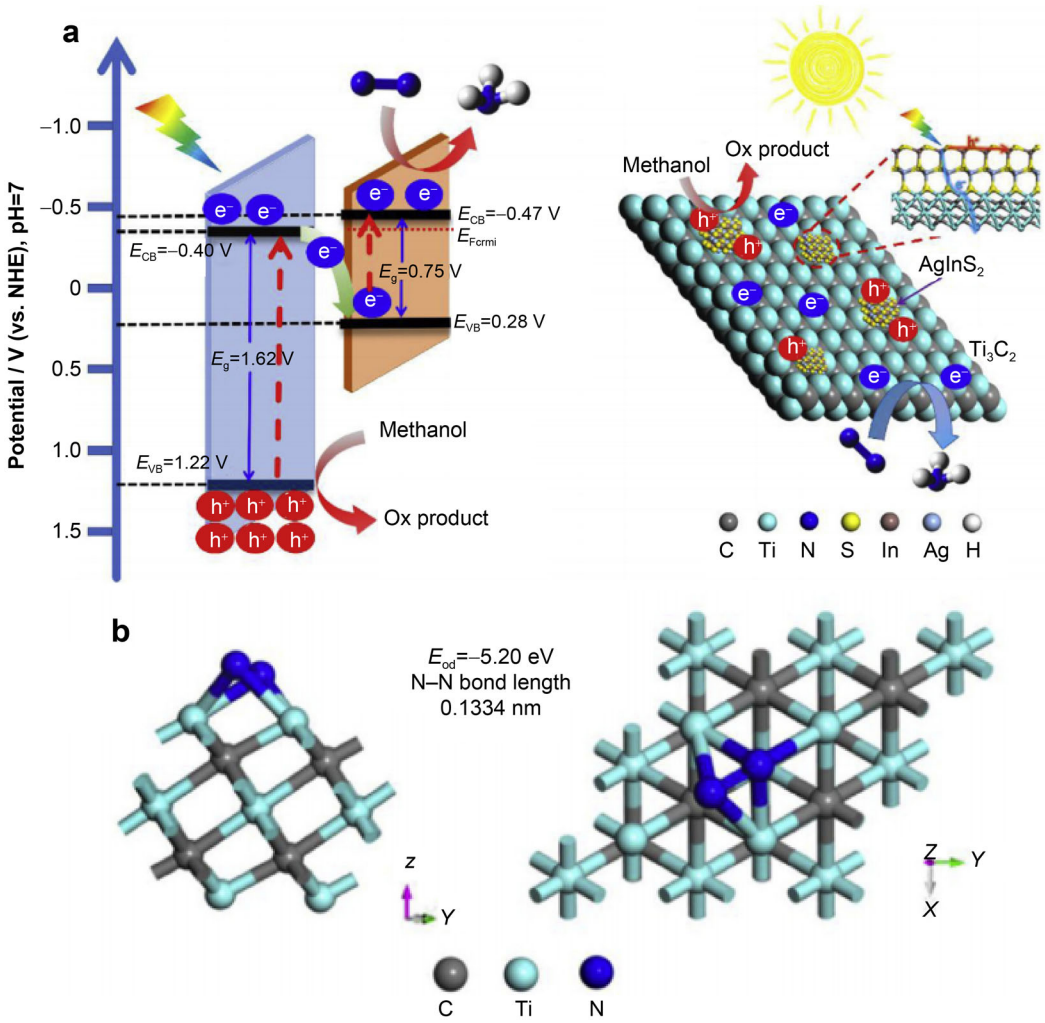

Fig. 18 Application of Ti_3C_2 in nitrogen photofixation. **a** Scheme for spatial charge separation and transportation during photocatalytic N_2 reduction over $AgInS_2/Ti_3C_2$ nanosheets; **b** adsorption configuration of N_2 molecule on Ti_3C_2 (001) surface with a ($2 \times 2 \times 1$) supercell and its corresponding N–N bond length. Reproduced with permission from Ref. [131]. Copyright 2019, Elsevier

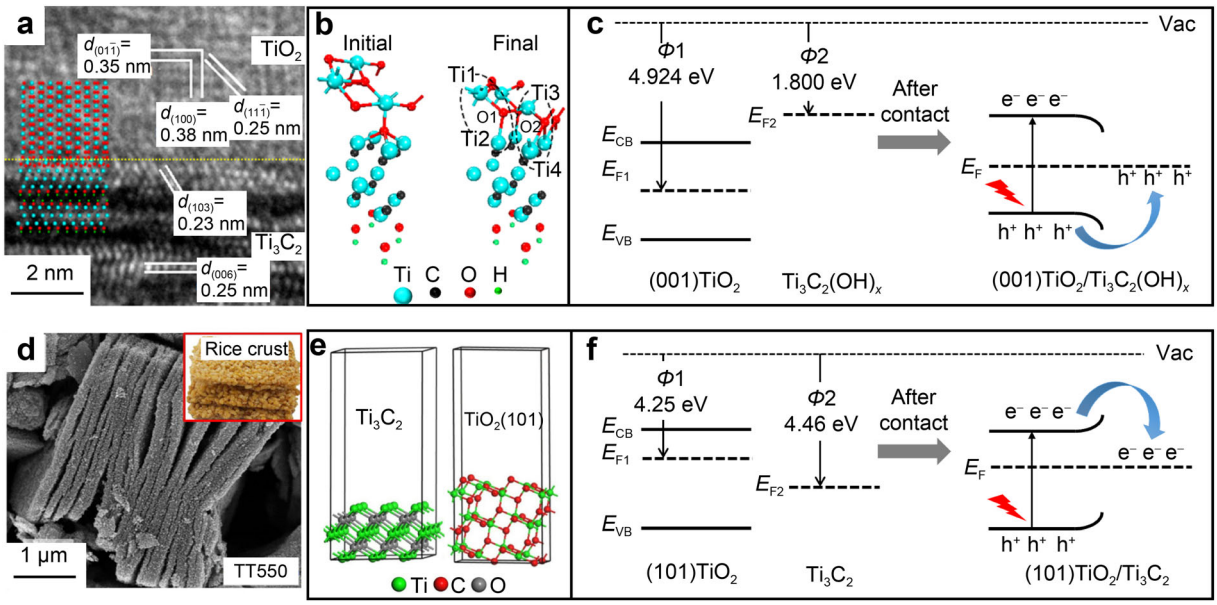

Fig. 19 Comparison of charge transfer mechanisms in TiO_2/Ti_3C_2 composites in different situations. **a** HRTEM image and (inset) model structure of TiO_2/Ti_3C_2 interface; **b** initial and final optimized interface structures of (001)TiO_2/OH-terminated Ti_3C_2 simulated by DFT; **c** energy level diagram of TiO_2/ Ti_3C_2 composite before and after contact, and formation mechanism of Schottky junction for holes trapping. Reproduced with permission from Ref. [58]. Copyright 2016, American Chemical Society. **d** SEM image of rice crust-like TiO_2/Ti_3C_2 composite; **e** schematic illustration for electronic structure of Ti_3C_2 and (101) facets of anatase TiO_2; **f** energy level diagram of TiO_2/Ti_3C_2 composite before and after contact, and formation mechanism of Schottky junction for electrons trapping. Reproduced with permission from Ref. [50]. Copyright 2018, Elsevier

In addition, the abundant groups located on the surface of $Ti_3C_2T_x$ endow it with intrinsic hydrophilicity, which makes it possible to achieve uniform dispersion in aqueous solution for those reactions occurred in aqueous systems. Furthermore, polymers, organic molecules, and inorganic nanomaterials can achieve the functionalization of $Ti_3C_2T_x$ through electrostatic physical adsorption or surface chemistry strategies.

(2) Adjustable forms of $Ti_3C_2T_x$ MXene make it adaptable to different needs. First, the accordion-like multilayered structure of $Ti_3C_2T_x$ is conducive to multiple reflections of electromagnetic waves, increasing energy consumption and improving electromagnetic wave absorption and shielding capabilities. After delamination, $Ti_3C_2T_x$ can exist in a few-layer/monolayer form, which offers a large specific surface area and thus abundant active sites for reactions. Therefore, it hides huge development potential in energy conversion and storage, wearable smart devices, and biomedicine. After further regulation, $Ti_3C_2T_x$ can be presented in the form of quantum dots, which is characteristic by fluorescence emission due to quantum size effect. The unique optical properties not only make $Ti_3C_2T_x$ show its brilliance in the field of biomedicine, but also have positive influence on the wide applications of $Ti_3C_2T_x$ in optical-related fields.

(3) Besides, $Ti_3C_2T_x$ possesses the special skill of light-to-heat conversion capability, which makes MXene widely favored in the fields of biomedicine, sensor, and energy conversion.

(4) Owing to the appropriate band structure and excellent conductivity, $Ti_3C_2T_x$ plays the role of co-catalyst in the field of photocatalysis by improving the carrier transport efficiency. Also, it can serve as an electrode material to enhance the energy storage capacity and optimize the sensitivity of the device in the sensor.

Hitherto, despite the fact that many efforts have been implemented in the research of $Ti_3C_2T_x$ and its composites, there are still several key points to be solved.

(1) Owing to the limitations of the preparation process through wet chemical etching, bare Ti_3C_2 without terminal surface groups has not yet been obtained. These difficult-to-control end groups will influence the electro-conductivity and surface properties of $Ti_3C_2T_x$ to a certain extent, which in turn affects its application scale. Besides, $Ti_3C_2T_x$ is easily oxidized in a humid environment, which will result in inevitable structural collapse and performance decline or even disappearance. Therefore, exploring a new

and smart strategy for preparing bare Ti_3C_2 is still a huge challenge.

(2) So far, most of the methods for preparing $Ti_3C_2T_x$ still rely on highly corrosive acid solutions. The utilization of these reagents will cause adverse effects on human body as well as environment. To this end, the exploitation of novel, polluting-free and non-toxic preparation strategies still needs a lot of attention. Moreover, except for the preparation of $Ti_3C_2T_x$ by selective etching MAX from up to bottom, the bottom-to-up fabrication technology has not yet been achieved, that is directly synthesizing $Ti_3C_2T_x$ from single atoms.

(3) As the current researches on the properties of $Ti_3C_2T_x$ are not sufficient, the reaction mechanism of $Ti_3C_2T_x$ in various application fields is still unclear and uncertain. Subsequent research could take advantage of theory calculation to interpret the true role of $Ti_3C_2T_x$ in the composite materials.

(4) Although $Ti_3C_2T_x$ has been clinically proven to be harmless to living organisms, its application in biomedical fields is still in its infancy. Especially, the long-term life safety of $Ti_3C_2T_x$ needs to be further confirmed.

(5) Concerning technical issues for mass production and process integration, most of the current research is limited to the laboratory, and has not been able to test in actual conditions. There is still a long way to go to commercialize $Ti_3C_2T_x$ and $Ti_3C_2T_x$-based composites.

Although the research on Ti_3C_2 and its composites is still in initial stage and many unknowns lie ahead, it is unable to conceal its enormous potential in diverse practical areas. Just keep our passion and faith in scientific knowledge, and it is hoped that this review can give some useful guidance to researchers in the related fields and pave the way for further development of MXene-based composites with bright prospect.

Acknowledgements This study was financially supported by the National Natural Science Foundation of China (No. 21972171) and Hubei Provincial Natural Science Foundation, China (No. 2021CFA022).

Declarations

Conflict of interests The authors declare that they have no conflict of interest.

References

[1] Novoselov KS, Geim AK, Morozov SV, Jiang D, Zhang Y, Dubonos SV, Grigorieva IV, Firsov AA. Electric field effect in atomically thin carbon films. Science. 2004;306(5696):666. https://doi.org/10.1126/science.1102896.

[2] Lalmi B, Oughaddou H, Enriquez H, Kara A, Vizzini S, Ealet B, Aufray B. Epitaxial growth of a silicene sheet. Appl Phys Lett. 2010;97(22):223109. https://doi.org/10.1063/1.3524215.

[3] Dávila M, Xian L, Cahangirov S, Rubio A, Le Lay G. Germanene: a novel two-dimensional germanium allotrope akin to graphene and silicene. New J Phys. 2014;16(9):095002. https://doi.org/10.1088/1367-2630/16/9/095002.

[4] Liu H, Neal A, Zhu Z, Luo Z, Xu X, Tomanek D, Ye P. Phosphorene: an unexplored 2D semiconductor with a high hole mobility. ACS Nano. 2014;8(4):4033. https://doi.org/10.1021/nn501226z.

[5] Ataca C, Şahin H, Ciraci S. Stable, single-layer MX_2 transition-metal oxides and dichalcogenides in a honeycomb-like structure. J Phys Chem C. 2012;116(16):8983. https://doi.org/10.1021/jp212558p.

[6] Coleman JN, Lotya M, O'neill A, Bergin SD, King PJ, Khan U, Young K, Gaucher A, De S, Smith RJ, Shvets IV, Arora SK, Stanton G, Kim HY, Lee K, Kim GT, Duesberg GS, Hallam T, Boland JJ, Wang JJ, Donegan JF, Grunlan JC, Moriarty G, Shmeliov A, Nicholls RJ, Perkins JM, Grieveson EM, Theuwissen K, Mccomb DW, Nellist PD, Nicolosi V. Liquid exfoliation of layered materials. Science. 2011;331(6017):568. https://doi.org/10.1126/science.1194975.

[7] Naguib M, Kurtoglu M, Presser V, Lu J, Niu J, Heon M, Hultman L, Gogotsi Y, Barsoum MW. Two-dimensional nanocrystals produced by exfoliation of Ti_3AlC_2. Adv Mater. 2011;23(37):4248. https://doi.org/10.1002/adma.201102306.

[8] Naguib M, Mashtalir O, Carle J, Presser V, Lu J, Hultman L, Gogotsi Y, Barsoum MW. Two-dimensional transition metal carbides. ACS Nano. 2012;6(2):1322. https://doi.org/10.1021/nn204153h.

[9] Anasori B, Xie Y, Beidaghi M, Lu J, Hosler B, Hultman L, Kent P, Gogotsi Y, Barsoum M. Two-dimensional, ordered, double transition metals carbides (MXenes). ACS Nano. 2015;9(10):9507. https://doi.org/10.1021/acsnano.5b03591.

[10] Huang K, Li Z, Lin J, Han G, Huang P. Two-dimensional transition metal carbides and nitrides (MXenes) for biomedical applications. Chem Soc Rev. 2018;47(14):5109. https://doi.org/10.1039/c7cs00838d.

[11] Naguib M, Mochalin V, Barsoum M, Gogotsi Y. 25th anniversary article: MXenes: a new family of two-dimensional materials. Adv Mater. 2014;26(7):992. https://doi.org/10.1002/adma.201304138.

[12] Mashtalir O, Naguib M, Mochalin VN, Dall'agnese Y, Heon M, Barsoum MW, Gogotsi Y. Intercalation and delamination of layered carbides and carbonitrides. Nat Commun. 2013;4:1716. https://doi.org/10.1038/ncomms2664.

[13] Han F, Luo S, Xie L, Zhu J, Wei W, Chen X, Liu F, Chen W, Zhao J, Dong L, Yu K, Zeng X, Rao F, Wang L, Huang Y. Boosting the yield of MXene 2D sheets via a facile hydrothermal-assisted intercalation. ACS Appl Mater Interfaces. 2019;11(8):8443. https://doi.org/10.1021/acsami.8b22339.

[14] Cai X, Luo Y, Liu B, Cheng H. Preparation of 2D material dispersions and their applications. Chem Soc Rev. 2018;47(16):6224. https://doi.org/10.1039/c8cs00254a.

[15] Yang C, Tan QY, Li Q, Zhou J, Fand JJ, Lie B, Suna J, Lv KL. Ti_3C_2 MXene/g-C_3N_4 nanosheets heterojunction for high efficient CO_2 reduction photocatalyst: dual effects of urea. Appl Catal B Environ. 2020;268:118738. https://doi.org/10.1016/j.apcatb.2020.118738.

[16] Lipatov A, Alhabeb M, Lukatskaya M, Boson A, Gogotsi Y, Sinitskii A. Effect of synthesis on quality, electronic properties and environmental stability of individual monolayer Ti_3C_2

MXene flakes. Adv Electron Mater. 2016;2(12):1600255. https://doi.org/10.1002/aelm.201600255.

[17] Xue Q, Zhang H, Zhu M, Pei Z, Li H, Wang Z, Huang Y, Huang Y, Deng Q, Zhou J, Du S, Huang Q, Zhi C. Photoluminescent Ti_3C_2 MXene quantum dots for multicolor cellular imaging. Adv Mater. 2017;29(15):1604847. https://doi.org/10.1002/adma.201604847.

[18] Xu G, Niu Y, Yang X, Jin Z, Wang Y, Xu Y, Niu H. Preparation of $Ti_3C_2T_x$ MXene-derived quantum dots with white/blue-emitting photoluminescence and electrochemiluminescence. Adv Opt Mater. 2018;6(24):1800951. https://doi.org/10.1002/adom.201800951.

[19] Zhang T, Jiang X, Li G, Yao Q, Lee J. A red-phosphorous-assisted ball-milling synthesis of few-layered $Ti_3C_2T_x$(MXene) nanodot composite. ChemNanoMat. 2018;4(1):56. https://doi.org/10.1002/cnma.201700232.

[20] Li XS, Liu F, Huang DP, Xue N, Dang YY, Zhang MQ, Zhang LL, Li B, Liu D, Wang L, Liu H, Tao XT. Nonoxidized MXene quantum dots prepared by microexplosion method for cancer catalytic therapy. Adv Funct Mater. 2020;30(24):2000308. https://doi.org/10.1002/adfm.202000308.

[21] Tang R, Xiong S, Gong D, Deng Y, Wang Y, Su L, Ding C, Yang L, Liao C. Ti_3C_2 2D MXene: recent progress and perspectives in photocatalysis. ACS Appl Mater Interfaces. 2020;12(51):56663. https://doi.org/10.1021/acsami.0c12905.

[22] Pang J, Mendes RG, Bachmatiuk A, Zhao L, Ta HQ, Gemming T, Liu H, Liu Z, Rummeli MH. Applications of 2D MXenes in energy conversion and storage systems. Chem Soc Rev. 2019;48(1):72. https://doi.org/10.1039/c8cs00324f.

[23] Wang H, Wu Y, Zhang J, Li G, Huang H, Zhang X, Jiang Q. Enhancement of the electrical properties of MXene Ti_3C_2 nanosheets by post-treatments of alkalization and calcination. Mater Lett. 2015;160(1):537. https://doi.org/10.1016/j.matlet.2015.08.046.

[24] Li ZP, Huang WX, Liu JX, Lv KL, Li Q. Embedding CdS@Au into ultrathin $Ti_{3-x}C_2T_y$ to build dual Schottky barriers for photocatalytic H_2 production. ACS Catal. 2021;11(14):8510. https://doi.org/10.1021/acscatal.1c02018.

[25] Zhao D, Chen Z, Yang W, Liu S, Zhang X, Yu Y, Cheong WC, Zheng L, Ren F, Ying G, Cao X, Wang D, Peng Q, Wang G, Chen C. MXene (Ti_3C_2) vacancy-confined single-atom catalyst for efficient functionalization of CO_2. J Am Chem Soc. 2019;141(9):4086. https://doi.org/10.1021/jacs.8b13579.

[26] Meng F, Seredych M, Chen C, Gura V, Mikhalovsky S, Sandeman S, Ingavle G, Ozulumba T, Miao L, Anasori B, Gogotsi Y. MXene sorbents for removal of urea from dialysate: a step toward the wearable artificial kidney. ACS Nano. 2018;12(10):10518. https://doi.org/10.1021/acsnano.8b06494.

[27] Wang H, Zhao R, Qin J, Hu H, Fan X, Cao X, Wang D. MIL-100(Fe)/Ti_3C_2 MXene as a Schottky catalyst with enhanced photocatalytic oxidation for nitrogen fixation activities. ACS Appl Mater Interfaces. 2019;11(47):44249. https://doi.org/10.1021/acsami.9b14793.

[28] Zhao Y, Zuo G, Wang Y, Teo WL, Xie A, Guo Y, Dai Y, Zhou W, Jana D, Xian Q, Dong W. Ultrathin $ZnIn_2S_4$ nanosheets anchored on $Ti_3C_2T_x$ MXene for photocatalytic H_2 evolution. Angew Chem Int Ed Engl. 2020;59(28):11287. https://doi.org/10.1002/anie.202002136.

[29] An H, Habib T, Shah S, Gao H, Patel A, Echols I, Zhao X, Radovic M, Green MJ, Lutkenhaus JL. Water sorption in MXene/polyelectrolyte multilayers for ultrafast humidity sensing. ACS Appl Nano Mater. 2019;2(2):948. https://doi.org/10.1021/acsanm.8b02265.

[30] Cao M, Cai Y, He P, Shu J, Cao W, Yuan J. 2D MXenes: electromagnetic property for microwave absorption and electromagnetic interference shielding. Chem Eng J. 2019;359:1265. https://doi.org/10.1016/j.cej.2018.11.051.

[31] Wang K, Lou Z, Wang L, Zhao L, Zhao S, Wang D, Han W, Jiang K, Shen G. Bioinspired interlocked structure-induced high deformability for two-dimensional titanium carbide (MXene)/natural microcapsule-based flexible pressure sensors. ACS Nano. 2019;13(8):9139. https://doi.org/10.1021/acsnano.9b03454.

[32] Wang Z, Yu K, Gong S, Mao H, Huang R, Zhu Z. Cu_3BiS_3/MXenes with excellent solar-thermal conversion for continuous and efficient seawater desalination. ACS Appl Mater Interfaces. 2021;13(14):16246. https://doi.org/10.1021/acsami.0c22761.

[33] Peng C, Wang H, Yu H, Peng F. (111) TiO_{2-x} /Ti_3C_2: synergy of active facets, interfacial charge transfer and Ti^{3+} doping for enhance photocatalytic activity. Mater Res Bull. 2017;89:16. https://doi.org/10.1016/j.materresbull.2016.12.049.

[34] Peng C, Wei P, Li X, Liu Y, Cao Y, Wang H, Yu H, Peng F, Zhang L, Zhang B, Lv K. High efficiency photocatalytic hydrogen production over ternary Cu/TiO_2@$Ti_3C_2T_x$ enabled by low-work-function 2D titanium carbide. Nano Energy. 2018;53:97. https://doi.org/10.1016/j.nanoen.2018.08.040.

[35] Wang H, Sun Y, Wu Y, Tu W, Wu S, Yuan X, Zeng G, Xu ZJ, Li S, Chew JW. Electrical promotion of spatially photoinduced charge separation via interfacial-built-in quasi-alloying effect in hierarchical $Zn_2In_2S_5$/Ti_3C_2(O, OH)$_x$ hybrids toward efficient photocatalytic hydrogen evolution and environmental remediation. Appl Catal B Environ. 2019;245:290. https://doi.org/10.1016/j.apcatb.2018.12.051.

[36] Cao S, Shen B, Tong T, Fu J, Yu J. 2D/2D heterojunction of ultrathin MXene/Bi_2WO_6 nanosheets for improved photocatalytic CO_2 reduction. Adv Funct Mater. 2018;28(21):1800136. https://doi.org/10.1002/adfm.201800136.

[37] Ran J, Gao G, Li F, Ma T, Du A, Qiao S. Ti_3C_2 MXene co-catalyst on metal sulfide photo-absorbers for enhanced visible-light photocatalytic hydrogen production. Nat Commun. 2017;8:13907. https://doi.org/10.1038/ncomms13907.

[38] Yang Q, Huang Z, Li X, Liu Z, Li H, Liang G, Wang D, Huang Q, Zhang S, Chen S, Zhi C. A wholly degradable, rechargeable Zn-Ti_3C_2 MXene capacitor with superior anti-self-discharge function. ACS Nano. 2019;13(7):8275. https://doi.org/10.1021/acsnano.9b03650.

[39] Zeng ZP, Yan YB, Chen J, Zan P, Tian QH, Chen P. Boosting the photocatalytic ability of Cu_2O nanowires for CO_2 conversion by MXene quantum dots. Adv Funct Mater. 2019;29(2):1806500. https://doi.org/10.1002/adfm.201806500.

[40] Lu Y, Fan DQ, Xu HL, Min HH, Lu CH, Lin ZX, Yang XF. Implementing hybrid energy harvesting in 3D spherical evaporator for solar steam generation and synergic water purification. Sol RRL. 2020;4(9):2000232. https://doi.org/10.1002/solr.202000232.

[41] Li X, Yin X, Han M, Song C, Xu H, Hou Z, Zhang L, Cheng L. Ti_3C_2 MXenes modified with in-situ grown carbon nanotubes for enhanced electromagnetic wave absorption properties. J Mater Chem C. 2017;5(16):4068. https://doi.org/10.1039/C6TC05226F.

[42] Gan R, Liu Y, Yang N, Tong C, Deng M, Dong Q, Tang X, Fu N, Li C, Wei Z. Lithium electrodeposited on lithiophilic LTO/Ti_3C_2 substrate as a dendrite-free lithium metal anode. J Mater Chem A. 2020;8(39):20650. https://doi.org/10.1039/d0ta07552c.

[43] Xie X, Zhao M, Anasori B, Maleski K, Ren C, Li J, Byles B, Pomerantseva E, Wang G, Gogotsi Y. Porous heterostructured MXene/carbon nanotube composite paper with high volumetric capacity for sodium-based energy storage devices. Nano

Energy. 2016;26:513. https://doi.org/10.1016/j.nanoen.2016.06.005.
[44] Wu G, Li T, Wang Z, Li M, Wang B, Dong A. Molecular ligand-mediated assembly of multicomponent nanosheet superlattices for compact capacitive energy storage. Angew Chem Int Ed Engl. 2020;59(46):20628. https://doi.org/10.1002/anie.202009086.
[45] Wang X, Wang J, Qin J, Xie X, Yang R, Cao M. Surface charge engineering for covalently assembling three-dimensional MXene network for all-climate sodium ion batteries. ACS Appl Mater Interfaces. 2020;12(35):39181. https://doi.org/10.1021/acsami.0c10605.
[46] Guo Q, Zhang X, Zhao F, Song Q, Su G, Tan Y, Tao Q, Zhou T, Yu Y, Zhou Z, Lu C. Protein-inspired self-healable Ti_3C_2 MXenes/rubber-based supramolecular elastomer for intelligent sensing. ACS Nano. 2020;14(3):2788. https://doi.org/10.1021/acsnano.9b09802.
[47] Weng G, Li J, Alhabeb M, Karpovich C, Wang H, Lipton J, Maleski K, Kong J, Shaulsky E, Elimelech M, Gogotsi Y, Taylor AD. Layer-by-layer assembly of cross-functional semi-transparent MXene-carbon nanotubes composite films for next-generation electromagnetic interference shielding. Adv Funct Mater. 2018;28(44):1803360. https://doi.org/10.1002/adfm.201803360.
[48] He F, Zhu BC, Cheng B, Yu JG, Ho W, Macyk W. 2D/2D/0D $TiO_2/C_3N_4/Ti_3C_2$ MXene composite S-scheme photocatalyst with enhanced CO_2 reduction activity. Appl Catal B Environ. 2020;272:119006. https://doi.org/10.1016/j.apcatb.2020.119006.
[49] Xing C, Chen S, Liang X, Liu Q, Qu M, Zou Q, Li J, Tan H, Liu L, Fan D, Zhang H. Two-dimensional MXene (Ti_3C_2)-integrated cellulose hydrogels: toward smart three-dimensional network nanoplatforms exhibiting light-induced swelling and bimodal photothermal/chemotherapy anticancer activity. ACS Appl Mater Interfaces. 2018;10(33):27631. https://doi.org/10.1021/acsami.8b08314.
[50] Low J, Zhang L, Tong T, Shen B, Yu J. TiO_2/MXene Ti_3C_2 composite with excellent photocatalytic CO_2 reduction activity. J Catal. 2018;361:255. https://doi.org/10.1016/j.jcat.2018.03.009.
[51] Liang R, Li Y, Huo M, Lin H, Chen Y. Triggering sequential catalytic fenton reaction on 2D MXenes for hyperthermia-augmented synergistic nanocatalytic cancer therapy. ACS Appl Mater Interfaces. 2019;11(46):42917. https://doi.org/10.1021/acsami.9b13598.
[52] Zou G, Zhang Z, Guo J, Liu B, Zhang Q, Fernandez C, Peng Q. Synthesis of MXene/Ag composites for extraordinary long cycle lifetime lithium storage at high rates. ACS Appl Mater Interfaces. 2016;8(34):22280. https://doi.org/10.1021/acsami.6b08089.
[53] Shi H, Zhang CJ, Lu P, Dong Y, Wen P, Wu ZS. Conducting and lithiophilic MXene/graphene framework for high-capacity, dendrite-free lithium-metal anodes. ACS Nano. 2019;13(12):14308. https://doi.org/10.1021/acsnano.9b07710.
[54] Chang T, Zhang T, Yang H, Li K, Tian Y, Lee J, Chen P. Controlled crumpling of two-dimensional titanium carbide (MXene) for highly stretchable, bendable, efficient supercapacitors. ACS Nano. 2018;12(8):8048. https://doi.org/10.1021/acsnano.8b02908.
[55] Ma C, Cao WT, Zhang W, Ma MG, Sun WM, Zhang J, Chen F. Wearable, ultrathin and transparent bacterial celluloses/MXene film with Janus structure and excellent mechanical property for electromagnetic interference shielding. Chem Eng J. 2021;403:126438. https://doi.org/10.1016/j.cej.2020.126438.
[56] Li ZM, Dall'agnese Y, Guo J, Huang HF, Liang XQ, Xu SK. Flexible freestanding all-MXene hybrid films with enhanced capacitive performance for powering a flex sensor. J Mater Chem A. 2020;8(32):16649. https://doi.org/10.1039/d0ta05710j.
[57] Zhou Z, Song Q, Huang B, Feng S, Lu C. Facile fabrication of densely packed Ti_3C_2 MXene/nanocellulose composite films for enhancing electromagnetic interference shielding and electro-/photothermal performance. ACS Nano. 2021;15:12405. https://doi.org/10.1021/acsnano.1c04526.
[58] Peng C, Yang X, Li Y, Yu H, Wang H, Peng F. Hybrids of two-dimensional Ti_3C_2 and TiO_2 exposing 001 facets toward enhanced photocatalytic activity. ACS Appl Mater Interfaces. 2016;8(9):6051. https://doi.org/10.1021/acsami.5b11973.
[59] Khazaei M, Ranjbar A, Arai M, Sasaki T, Yunoki S. Electronic properties and applications of MXenes: a theoretical review. J Mater Chem C. 2017;5(10):2488. https://doi.org/10.1039/c7tc00140a.
[60] Zhao M, Ren C, Ling Z, Lukatskaya M, Zhang C, Van Aken K, Barsoum M, Gogotsi Y. Flexible MXene/carbon nanotube composite paper with high volumetric capacitance. Adv Mater. 2015;27(2):339. https://doi.org/10.1002/adma.201404140.
[61] Lin H, Chen L, Lu X, Yao H, Chen Y, Shi J. Two-dimensional titanium carbide MXenes as efficient non-noble metal electrocatalysts for oxygen reduction reaction. Sci China Mater. 2018;62(5):662. https://doi.org/10.1007/s40843-018-9378-3.
[62] Wang Z, Xuan J, Zhao Z, Li Q, Geng F. Versatile cutting method for producing fluorescent ultrasmall MXene sheets. ACS Nano. 2017;11(11):11559. https://doi.org/10.1021/acsnano.7b06476.
[63] Wang XL, Wang LB, He Y, Wu M, Zhou AG. The effect of two-dimensional d-Ti_3C_2 on the mechanical and thermal conductivity properties of thermoplastic polyurethane composites. Polym Compos. 2019;41(1):350. https://doi.org/10.1002/pc.25374.
[64] Feng YF, Zhou FR, Deng QI, Peng C. Solvothermal synthesis of in situ nitrogen-doped Ti_3C_2 MXene fluorescent quantum dots for selective Cu^{2+} detection. Ceram Int. 2020;46(6):8320. https://doi.org/10.1016/j.ceramint.2019.12.063.
[65] Tao N, Liu YD, Wu YJ, Li XL, Li J, Sun XY, Chen S, Liu Y. Minimally invasive antitumor therapy using biodegradable nanocomposite micellar hydrogel with functionalities of NIR-II photothermal ablation and vascular disruption. ACS Appl Bio Mater. 2020;3(7):4531. https://doi.org/10.1021/acsabm.0c00465.
[66] Wang X, Shen X, Gao Y, Wang Z, Yu R, Chen L. Atomic-scale recognition of surface structure and intercalation mechanism of Ti_3C_2X. J Am Chem Soc. 2015;137(7):2715. https://doi.org/10.1021/ja512820k.
[67] Li Q, Zhong B, Zhang W, Jia Z, Jia D, Qin S, Wang J, Razal JM, Wang X. Ti_3C_2 MXene as a new nanofiller for robust and conductive elastomer composites. Nanoscale. 2019;11(31):14712. https://doi.org/10.1039/c9nr03661j.
[68] Sheng XX, Li SH, Huang HW, Zhao YF, Chen Y, Zhang L, Xie DL. Anticorrosive and UV-blocking waterborne polyurethane composite coating containing novel two-dimensional Ti_3C_2 MXene nanosheets. J Mater Sci. 2020;56(6):4212. https://doi.org/10.1007/s10853-020-05525-2.
[69] Ng VM, Huang H, Zhou K, Lee P, Que W, Xu JZ, Kong L. Recent progress in layered transition metal carbides and/or nitrides (MXenes) and their composites: synthesis and applications. J Mater Chem A. 2017;5(7):3039. https://doi.org/10.1039/C6TA06772G.
[70] Yang S, Zhang P, Wang F, Ricciardulli A, Lohe M, Blom PWM, Feng X. Fluoride-free synthesis of two-dimensional titanium carbide (MXene) using a binary aqueous system. Angew Chem Int Ed Engl. 2018;57(47):15491. https://doi.org/10.1002/anie.201809662.

[71] Lukatskaya M, Kota S, Lin Z, Zhao M, Shpigel N, Levi M, Halim J, Taberna P, Barsoum M, Simon P, Gogotsi Y. Ultra-high-rate pseudocapacitive energy storage in two-dimensional transition metal carbides. Nat Energy. 2017;2:17105. https://doi.org/10.1038/nenergy.2017.105.

[72] Zhang JZ, Kong N, Uzun S, Levitt A, Seyedin S, Lynch PA, Qin S, Han MK, Yang WR, Liu JQ, Wang XG, Gogotsi Y, Razal JM. Scalable manufacturing of free-standing, strong $Ti_3C_2T_x$ MXene films with outstanding conductivity. Adv Mater. 2020;32(23):e2001093. https://doi.org/10.1002/adma.202001093.

[73] De S, King PJ, Lotya M, O'neill A, Doherty EM, Hernandez Y, Duesberg GS, Coleman JN. Flexible, transparent, conducting films of randomly stacked graphene from surfactant-stabilized, oxide-free graphene dispersions. Small. 2010;6(3):458. https://doi.org/10.1002/smll.200901162.

[74] Hantanasirisakul K, Alhabeb M, Lipatov A, Maleski K, Anasori B, Salles P, Ieosakulrat C, Pakawatpanurut P, Sinitskii A, May SJ, Gogotsi Y. Effects of synthesis and processing on optoelectronic properties of titanium carbonitride MXene. Chem Mater. 2019;31(8):2941. https://doi.org/10.1021/acs.chemmater.9b00401.

[75] Hart JL, Hantanasirisakul K, Lang AC, Anasori B, Pinto D, Pivak Y, Van Omme JT, May SJ, Gogotsi Y, Taheri ML. Control of MXenes' electronic properties through termination and intercalation. Nat Commun. 2019;10:1. https://doi.org/10.1038/s41467-018-08169-8.

[76] Muckley ES, Naguib M, Wang HW, Vlcek L, Osti NC, Sacci RL, Sang XH, Unocic RR, Xie Y, Tyagi M, Mamontov E, Page KL, Kent PRC, Nanda J, Ivanov IN. Multimodality of structural, electrical, and gravimetric responses of intercalated MXenes to water. ACS Nano. 2017;11(11):11118. https://doi.org/10.1021/acsnano.7b05264.

[77] Halim J, Lukatskaya M, Cook K, Lu J, Smith C, Naslund L, May S, Hultman L, Gogotsi Y, Eklund P, Barsoum M. Transparent conductive two-dimensional titanium carbide epitaxial thin films. Chem Mater. 2014;26(7):2374. https://doi.org/10.1021/cm500641a.

[78] Bergmann G. Quantitative analysis of weak localization in thin Mg films by magnetoresistance measurements. Phys Rev B. 1982;25(4):2937. https://doi.org/10.1103/PhysRevB.25.2937.

[79] Cai T, Wang L, Liu Y, Zhang S, Dong W, Chen H, Yi X, Yuan J, Xia X, Liu C, Luo S. Ag_3PO_4/Ti_3C_2 MXene interface materials as a Schottky catalyst with enhanced photocatalytic activities and anti-photocorrosion performance. Appl Catal B Environ. 2018;239:545. https://doi.org/10.1016/j.apcatb.2018.08.053.

[80] Singh B, Bahadur R, Neekhra S, Gandhi M, Srivastava R. Hydrothermal-assisted synthesis and stability of multifunctional MXene nanobipyramids: structural, chemical, and optical evolution. ACS Appl Mater Interfaces. 2021;13(2):3011. https://doi.org/10.1021/acsami.0c18712.

[81] Zhang Q, Yi G, Fu Z, Yu H, Chen S, Quan X. Vertically aligned Janus MXene-based aerogels for solar desalination with high efficiency and salt resistance. ACS Nano. 2019;13(11):13196. https://doi.org/10.1021/acsnano.9b06180.

[82] Wang QW, Zhang HB, Liu J, Zhao S, Xie X, Liu LX, Yang R, Koratkar N, Yu ZZ. Multifunctional and water-resistant MXene-decorated polyester textiles with outstanding electromagnetic interference shielding and joule heating performances. Adv Funct Mater. 2019;29(7):1806819. https://doi.org/10.1002/adfm.201806819.

[83] Zhao JQ, Yang YW, Yang CH, Tian YP, Han Y, Liu J, Yin XT, Que WX. A hydrophobic surface enabled salt-blocking 2D Ti_3C_2 MXene membrane for efficient and stable solar desalination. J Mater Chem A. 2018;6(33):16196. https://doi.org/10.1039/c8ta05569f.

[84] Liu J, Zhang H, Sun R, Liu Y, Liu Z, Zhou A, Yu Z. Hydrophobic, flexible, and lightweight MXene foams for high-performance electromagnetic-interference shielding. Adv Mater. 2017;29(38):1702367. https://doi.org/10.1002/adma.201702367.

[85] Zhao XF, Vashisth A, Prehn E, Sun WM, Shah SA, Habib T, Chen YX, Tan ZY, Lutkenhaus JL, Radovic M, Green MJ. Antioxidants unlock shelf-stable $Ti_3C_2T_x$ (MXene) nanosheet dispersions. Matter. 2019;1(2):513. https://doi.org/10.1016/j.matt.2019.05.020.

[86] Maleski K, Mochalin VN, Gogotsi Y. Dispersions of two-dimensional titanium carbide MXene in organic solvents. Chem Mater. 2017;29(4):1632. https://doi.org/10.1021/acs.chemmater.6b04830.

[87] Zhang J, Kong N, Hegh D, Usman KAS, Guan G, Qin S, Jurewicz I, Yang W, Razal JM. Freezing titanium carbide aqueous dispersions for ultra-long-term storage. ACS Appl Mater Interfaces. 2020;12(30):34032. https://doi.org/10.1021/acsami.0c06728.

[88] Zhang C, Pinilla S, Mcevoy N, Cullen C, Anasori B, Long E, Park S-H, Seral-Ascaso A, Shmeliov A, Krishnan D, Morant C, Liu X, Duesberg GS, Gogotsi Y, Nicolosi V. Oxidation stability of colloidal two-dimensional titanium carbides (MXenes). Chem Mater. 2017;29(11):4848. https://doi.org/10.1021/acs.chemmater.7b00745.

[89] Habib T, Zhao X, Shah SA, Chen Y, Sun W, An H, Lutkenhaus JL, Radovic M, Green MJ. Oxidation stability of $Ti_3C_2T_x$ MXene nanosheets in solvents and composite films. NPJ 2D Mater Appl. 2019;3(1):1. https://doi.org/10.1038/s41699-019-0089-3.

[90] Yan J, Ma Y, Zhang C, Li X, Liu W, Yao X, Yao S, Luo S. Polypyrrole-MXene coated textile-based flexible energy storage device. Rsc Adv. 2018;8(69):39742. https://doi.org/10.1039/c8ra08403c.

[91] Lyu B, Kim M, Jing H, Kang J, Qian C, Lee S, Cho JH. Large-area MXene electrode array for flexible electronics. ACS Nano. 2019;13(10):11392. https://doi.org/10.1021/acsnano.9b04731.

[92] Firestein KL, Von Treifeldt JE, Kvashnin DG, Fernando JFS, Zhang C, Kvashnin AG, Podryabinkin EV, Shapeev AV, Siriwardena DP, Sorokin PB, Golberg D. Young's modulus and tensile strength of Ti_3C_2 MXene nanosheets as revealed by in situ TEM probing, AFM nanomechanical mapping, and theoretical calculations. Nano Lett. 2020;20:5900. https://doi.org/10.1021/acs.nanolett.0c01861.

[93] Akhlaghi M, Tayebifard SA, Salahi E, Shahedi Asl M, Schmidt G. Self-propagating high-temperature synthesis of Ti_3AlC_2 MAX phase from mechanically-activated Ti/Al/graphite powder mixture. Ceram Int. 2018;44(8):9671. https://doi.org/10.1016/j.ceramint.2018.02.195.

[94] Chen JX, Li ZL, Ni FL, Ouyang WX, Fang XS. Bio-inspired transparent MXene electrodes for flexible UV photodetectors. Mater Horiz. 2020;7:1828. https://doi.org/10.1039/d0mh00394h.

[95] Abdolhosseinzadeh S, Jiang XT, Zhang H, Qiu JS, Zhang CF. Perspectives on solution processing of two-dimensional MXenes. Mater Today. 2021;48:214. https://doi.org/10.1016/j.mattod.2021.02.010.

[96] Wang L, Zhang H, Wang B, Shen C, Zhang C, Hu Q, Zhou A, Liu B. Synthesis and electrochemical performance of $Ti_3C_2T_x$ with hydrothermal process. Electron Mater Lett. 2016;12(5):702. https://doi.org/10.1007/s13391-016-6088-z.

[97] Feng A, Yu Y, Wang Y, Jiang F, Yu Y, Mi L, Song L. Two-dimensional MXene Ti_3C_2 produced by exfoliation of

Ti_3AlC_2. Mater Des. 2017;114(15):161. https://doi.org/10.1016/j.matdes.2016.10.053.
[98] Xiu LY, Wang ZY, Qiu JS. General synthesis of MXene by green etching chemistry of fluoride-free Lewis acidic melts. Rare Met. 2020;39(11):1237. https://doi.org/10.1007/s12598-020-01488-0.
[99] Li Y, Shao H, Lin Z, Lu J, Liu L, Duployer B, Persson POA, Eklund P, Hultman L, Li M, Chen K, Zha XH, Du S, Rozier P, Chai Z, Raymundo-Pinero E, Taberna PL, Simon P, Huang Q. A general Lewis acidic etching route for preparing MXenes with enhanced electrochemical performance in non-aqueous electrolyte. Nat Mater. 2020;19:894. https://doi.org/10.1038/s41563-020-0657-0.
[100] Xie X, Xue Y, Li L, Chen S, Nie Y, Ding W, Wei Z. Surface Al leached Ti_3AlC_2 as a substitute for carbon for use as a catalyst support in a harsh corrosive electrochemical system. Nanoscale. 2014;6(19):11035. https://doi.org/10.1039/C4NR02080D.
[101] Chia HL, Mayorga-Martinez CC, Antonatos N, Sofer Z, Gonzalez-Julian JJ, Webster RD, Pumera M. MXene titanium carbide-based biosensor: strong dependence of exfoliation method on performance. Anal Chem. 2020;92(3):2452. https://doi.org/10.1021/acs.analchem.9b03634.
[102] Li N, Jiang Y, Zhou C, Xiao Y, Meng B, Wang Z, Huang D, Xing C, Peng Z. High-performance humidity sensor based on urchin-like composite of Ti_3C_2 MXene-derived TiO_2 nanowires. ACS Appl Mater Interfaces. 2019;11(41):38116. https://doi.org/10.1021/acsami.9b12168.
[103] Ghidiu M, Lukatskaya M, Zhao M, Gogotsi Y, Barsoum M. Conductive two-dimensional titanium carbide "clay" with high volumetric capacitance. Nature. 2014;516(7529):78. https://doi.org/10.1038/nature13970.
[104] Rafieerad A, Yan W, Sequiera GL, Sareen N, Abu-El-Rub E, Moudgil M, Dhingra S. Application of Ti_3C_2 MXene quantum dots for immunomodulation and regenerative medicine. Adv Healthcare Mater. 2019;8(16):e1900569. https://doi.org/10.1002/adhm.201900569.
[105] Shao BB, Liu ZF, Zeng GM, Wang H, Liang QH, He QY, Cheng M, Zhou CY, Jiang LB, Song B. Two-dimensional transition metal carbide and nitride (MXene) derived quantum dots (QDs): synthesis, properties, applications and prospects. J Mater Chem A. 2020;8(16):7508. https://doi.org/10.1039/d0ta01552k.
[106] Liu D, Zhang G, Ji Q, Zhang Y, Li J. Synergistic electrocatalytic nitrogen reduction enabled by confinement of nanosized Au particles onto a two-dimensional Ti_3C_2 substrate. ACS Appl Mater Interfaces. 2019;11(29):25758. https://doi.org/10.1021/acsami.9b02511.
[107] Su T, Hood ZD, Naguib M, Bai L, Luo S, Rouleau CM, Ivanov IN, Ji H, Qin Z, Wu Z. Monolayer $Ti_3C_2T_x$ as an effective co-catalyst for enhanced photocatalytic hydrogen production over TiO_2. ACS Appl Energy Mater. 2019;2(7):4640. https://doi.org/10.1021/acsaem.8b02268.
[108] Zhao QN, Zhang YJ, Duan ZH, Wang S, Liu C, Jiang YD, Tai HL. A review on $Ti_3C_2T_x$-based nanomaterials: synthesis and applications in gas and humidity sensors. Rare Met. 2021;40(6):1459. https://doi.org/10.1007/s12598-020-01602-2.
[109] Jiao S, Liu L. Friction-induced enhancements for photocatalytic degradation of MoS_2@Ti_3C_2 nanohybrid. Ind Eng Chem Res. 2019;58(39):18141. https://doi.org/10.1021/acs.iecr.9b03680.
[110] Chen Y, Wu G, Chen B, Qu H, Jiao T, Li Y, Ge C, Zhang C, Liang L, Zeng X, Cao X, Wang Q, Li H. Self-assembly of a purely covalent cage with homochirality by imine formation in water. Angew Chem Int Ed Engl. 2021;60(34):18815. https://doi.org/10.1002/anie.202106428.
[111] Hu XY, Yan LL, Wang YM, Xu M. Ice segregation induced self-assembly of salecan and grapheme oxide nanosheets into ion-imprinted aerogel with superior selectivity for cadmium (II) capture. Chem Eng J. 2021;417:128106. https://doi.org/10.1016/j.cej.2020.128106.
[112] Guo J, Zhao Y, Liu A, Ma T. Electrostatic self-assembly of 2D delaminated MXene (Ti_3C_2) onto Ni foam with superior electrochemical performance for supercapacitor. Electrochim Acta. 2019;305:164. https://doi.org/10.1016/j.electacta.2019.03.025.
[113] Li Z, Cui Y, Wu Z, Milligan C, Zhou L, Mitchell G, Xu B, Shi E, Miller JT, Ribeiro FH, Wu Y. Reactive metal–support interactions at moderate temperature in two-dimensional niobium-carbide-supported platinum catalysts. Nat Catal. 2018;1(5):349. https://doi.org/10.1038/s41929-018-0067-8.
[114] Ying Y, Liu Y, Wang X, Mao Y, Cao W, Hu P, Peng X. Two-dimensional titanium carbide for efficiently reductive removal of highly toxic chromium(VI) from water. ACS Appl Mater Interfaces. 2015;7(3):1795. https://doi.org/10.1021/am5074722.
[115] Zhang Z, Li H, Zou G, Fernandez C, Liu B, Zhang Q, Hu J, Peng Q. Self-reduction synthesis of new MXene/Ag composites with unexpected electrocatalytic activity. ACS Sustain Chem Eng. 2016;4(12):6763. https://doi.org/10.1021/acssuschemeng.6b01698.
[116] Han M, Yin X, Wu H, Hou Z, Song C, Li X, Zhang L, Cheng L. Ti_3C_2 MXenes with modified surface for high-performance electromagnetic absorption and shielding in the X-band. ACS Appl Mater Interfaces. 2016;8(32):21011. https://doi.org/10.1021/acsami.6b06455.
[117] Li R, Zhang L, Shi L, Wang P. MXene Ti_3C_2: an effective 2D light-to-heat conversion material. ACS Nano. 2017;11(4):3752. https://doi.org/10.1021/acsnano.6b08415.
[118] Liu G, Zou J, Tang Q, Yang X, Zhang Y, Zhang Q, Huang W, Chen P, Shao J, Dong X. Surface modified Ti_3C_2 MXene nanosheets for tumor targeting photothermal/photodynamic/chemo synergistic therapy. ACS Appl Mater Interfaces. 2017;9(46):40077. https://doi.org/10.1021/acsami.7b13421.
[119] Xuan J, Wang Z, Chen Y, Liang D, Cheng L, Yang X, Liu Z, Ma R, Sasaki T, Geng F. Organic-base-driven intercalation and delamination for the production of functionalized titanium carbide nanosheets with superior photothermal therapeutic performance. Angew Chem Int Ed. 2016;55:14569. https://doi.org/10.1002/anie.201606643.
[120] Lin H, Wang Y, Gao S, Chen Y, Shi J. Theranostic 2D tantalum carbide (MXene). Adv Mater. 2018;30(4):1703284. https://doi.org/10.1002/adma.201703284.
[121] Li M, Li X, Qin G, Luo K, Lu J, Li Y, Liang G, Huang Z, Zhou J, Hultman L, Eklund P, Persson POA, Du S, Chai Z, Zhi C, Huang Q. Halogenated Ti_3C_2 MXenes with electrochemically active terminals for high-performance zinc ion batteries. ACS Nano. 2021;15(1):1077. https://doi.org/10.1021/acsnano.0c07972.
[122] Cheng L, Li X, Zhang H, Xiang Q. Two-dimensional transition metal MXene-based photocatalysts for solar fuel generation. J Phys Chem Lett. 2019;10(12):3488. https://doi.org/10.1021/acs.jpclett.9b00736.
[123] You Z, Liao Y, Li X, Fan J, Xiang Q. State-of-the-art recent progress in MXene-based photocatalysts: a comprehensive review. Nanoscale. 2021;13(21):9463. https://doi.org/10.1039/d1nr02224e.
[124] Yang Y, Zhang D, Xiang Q. Plasma-modified $Ti_3C_2T_x$/CdS hybrids with oxygen-containing groups for high-efficiency photocatalytic hydrogen production. Nanoscale. 2019;11(40):18797. https://doi.org/10.1039/c9nr07242j.
[125] Ding M, Xiao R, Zhao C, Bukhvalov D, Chen Z, Xu H, Tang H, Xu J, Yang X. Evidencing interfacial charge transfer in 2D CdS/2D MXene Schottky heterojunctions toward

high-efficiency photocatalytic hydrogen production. Sol RRL. 2020;5(2):2000414. https://doi.org/10.1002/solr.202000414.
[126] Ding M, Han C, Yuan Y, Xu J, Yang X. Advances and promises of 2D MXenes as cocatalysts for artificial photosynthesis. Sol RRL. 2021;5(12):2100603. https://doi.org/10.1002/solr.202100603.
[127] Xiao R, Zhao C, Zou Z, Chen Z, Tian L, Xu H, Tang H, Liu Q, Lin Z, Yang X. In situ fabrication of 1D CdS nanorod/2D Ti_3C_2 MXene nanosheet Schottky heterojunction toward enhanced photocatalytic hydrogen evolution. Appl Catal B Environ. 2020;268:118382. https://doi.org/10.1016/j.apcatb.2019.118382.
[128] Norskov JK, Bligaard T, Rossmeisl J, Christensen CH. Towards the computational design of solid catalysts. Nat Chem. 2009;1(1):37. https://doi.org/10.1038/nchem.121.
[129] Jiao Y, Zheng Y, Jaroniec M, Qiao S. Design of electrocatalysts for oxygen- and hydrogen-involving energy conversion reactions. Chem Soc Rev. 2015;44(8):2060. https://doi.org/10.1039/c4cs00470a.
[130] Sang X, Xie Y, Lin M, Alhabeb M, Van Aken K, Gogotsi Y, Kent P, Xiao K, Unocic R. Atomic defects in monolayer titanium carbide ($Ti_3C_2T_x$) MXene. ACS Nano. 2016;10(10):9193. https://doi.org/10.1021/acsnano.6b05240.
[131] Qin J, Hu X, Li X, Yin Z, Liu B, Lam K-H. 0D/2D $AgInS_2$/MXene Z-scheme heterojunction nanosheets for improved ammonia photosynthesis of N_2. Nano Energy. 2019;61:27. https://doi.org/10.1016/j.nanoen.2019.04.028.
[132] Liao Y, Qian J, Xie G, Han Q, Dang W, Wang Y, Lv L, Zhao S, Luo L, Zhang W, Jiang H-Y, Tang J. 2D-layered Ti_3C_2 MXenes for promoted synthesis of NH_3 on P25 photocatalysts. Appl Catal B Environ. 2020;273(15):119054. https://doi.org/10.1016/j.apcatb.2020.119054.
[133] Sun B, Qiu P, Liang Z, Xue Y, Zhang X, Yang L, Cui H, Tian J. The fabrication of 1D/2D CdS nanorod@Ti_3C_2 MXene composites for good photocatalytic activity of hydrogen generation and ammonia synthesis. Chem Eng J. 2021;406(15):127177. https://doi.org/10.1016/j.cej.2020.127177.

Qin Li is currently an associate professor in the School of Chemistry and Materials Science, South-Central Minzu University, Wuhan, China. She received her B.S. and Ph.D. degrees in the major of Materials Science from Wuhan University of Technology in 2009 and 2014, respectively. Her major research activities are devoted to developing novel strategies for the enhanced photocatalytic hydrogen production performance over metal sulfide-based nanomaterials under visible-light irradiation.